4862 J. Med. Chem. 2010, 53, 4862–4876
DOI: 10.1021/jm100213c

Journal of Medicinal Chemistry Article

Mercaptophosphonate Compounds as Broad-Spectrum Inhibitors of the Metallo-β-lactamases†

Patricia Lassaux,[‡,∥] Matthieu Hamel,[⊥] Mihaela Gulea,[⊥] Heinrich Delbrück,[#] Paola Sandra Mercuri,[‡,∥] Louise Horsfall,[‡,∥] Dominique Dehareng,[§] Michaël Kupper,[#] Jean-Marie Frère,[∥] Kurt Hoffmann,[#] Moreno Galleni,[‡,∥] and Carine Bebrone*[,‡,∥]

[‡]*Laboratory of Biological Macromolecules,* [§]*Applied Quantum Chemistry and Molecular Modelling Unit, and* [∥]*Centre for Protein Engineering, University of Liège, Allée du 6 Août B6, Sart-Tilman, 4000 Liège, Belgium,* [⊥]*Laboratoire de Chimie Moléculaire et Thio-Organique, UMR CNRS 6507, INC3M, FR 3038, ENSICAEN, Université de Caen, 6, Boulevard du Maréchal Juin, 14 050 CAEN, France, and* [#]*Institute of Molecular Biotechnology, RWTH-Aachen University, c/o Fraunhofer IME, Forckenbeckstrasse 6, 52074 Aachen, Germany*

Received November 4, 2009

Although commercialized inhibitors of active site serine β-lactamases are currently used in coadministration with antibiotic therapy, no clinically useful inhibitors of metallo-β-lactamases (MBLs) have yet been discovered. In this paper, we investigated the inhibitory effect of mercaptophosphonate derivatives against the three subclasses of MBLs (B1, B2, and B3). All 14 tested mercaptophosphonates, with the exception of **1a**, behaved as competitive inhibitors for the three subclasses. Apart from **13** and **21**, all the mercaptophosphonates tested exhibit a good inhibitory effect on the subclass B2 MBL CphA with low inhibition constants ($K_i < 15\ \mu M$). Interestingly, compound **18** turned out to be a potent broad spectrum MBL inhibitor. The crystallographic structures of the CphA−**10a** and CphA−**18** complexes indicated that the sulfur atom of **10a** and the phosphonato group of **18** interact with the Zn^{2+} ion, respectively. Molecular modeling studies of the interactions between compounds **10a** and **18** and the VIM-4 (B1), CphA (B2), and FEZ-1 (B3) enzymes brought to light different binding modes depending on the enzyme and the inhibitor, consistent with the crystallographic structures.

Introduction

To withstand β-lactam antibiotics, bacteria are able to produce β-lactamases. Among these enzymes, the metallo-β-lactamase (MBL[a]) group represents an emerging problem because of its capacity to hydrolyze almost all β-lactam antibiotics, including last generation cephalosporins and carbapenems, and its capacity to propagate among nosocomial bacterial strains. MBLs constitute the class B of the β-lactamase family, whereas classes A, C, and D are composed of different serine active site enzymes.[1] On the basis of the known sequences, three different lineages of MBLs, identified as subclasses B1, B2, and B3, can be characterized.[2,3] Also, functional and mechanistic factors clearly distinguish the B1, B2, and B3 enzymes from each other.[4,5]

In parallel to the search for new non-β-lactamase-susceptible antibiotics, a second strategy to counter β-lactam resistance is to coadminister the β-lactam antibiotic with a β-lactamase inhibitor or inactivator. Commercialized inactivators are clavulanic acid, sulbactam, and tazobactam. Unfortunately, they are only active against serine β-lactamases and do not inactivate MBLs.[6] Several classes of MBLs inhibitors have already been described; however, none of these classes constitute the "ideal" MBL inhibitor.[5,7] The remaining challenge is thus to find a specific inhibitor of MBLs that is active on all three subclasses. Among the already described inhibitors, thiols and mercaptoacetic acid thiol esters were reported to be broad spectrum MBL inhibitors.[8−11] Indeed, thiomandelic acid was an efficient inhibitor ($K_i < 0.80\ \mu M$) of all the MBLs tested, with the exception of the subclass B2 CphA enzyme ($K_i = 244\ \mu M$).[8] The most potent broad spectrum MBL inhibitors contain both sulfanyl (thiolate) and carboxylate functional groups capable of metal ligation. The sulfanyl group was necessary for the inhibition of the enzyme, while the carboxylate group was not critical. A study based on the structure−activity relationship of inhibitors has emphasized the importance in the proximity of the sulfanyl group to the carboxylate group in enabling successful inhibition.[8] Therefore, because of the presence of two chelating functions (sulfanyl and phosphonato), the mercaptophosphonic acids (phosphorus analogues of mercaptocarboxylic acids) are potential candidates for MBL inhibitors. Since the work of Schwarzenbach in 1949, phosphonates and phosphonic acids were known as effective chelating agents.[12] Two reviews dealing with P,S-difunctionalized compounds showed their various applications (in biomolecular chemistry, catalysis, and hybrid materials chemistry), mainly arising from their metal-chelating properties.[13] Moreover, phosphonate monoesters are known to be inhibitors of active serine class A and C β-lactamases.[14,15] In 2005, inhibition of class D β-lactamases by phosphonates was also demonstrated.[16] However, to the best of our knowledge, only two publications described the use of mercaptophosphonic acids as metallophosphatase inhibitors.[17,18] Thus, a study of this class of compounds as promising inhibitors of MBLs seems to be required.

†PDB codes: 3IOF and 3IOG.

*To whom correspondence should be addressed. Phone: +3243663315. Fax: +3243663364. E-mail: carine.bebrone@ulg.ac.be.

[a] Abbreviations: IC_{50}, concentration of inhibitor leading to 50% inhibition; K_i, inhibition constant; MBL(s), metallo-β-lactamase(s); MM, molecular mechanics; MMP, mercaptomethylphosphonate; PAA, phosphoracetic acid; PDB, Protein Data Bank; rmsd, root mean square deviation; SAR, structure−activity relationship; THF, tetrahydrofuran; TLC, thin-layer chromatography; TLS, translation/libration/screw; TMS, tetramethylsilane; Zn1, the Zn^{2+} ion in the so-called "histidine" binding site; Zn2, the Zn^{2+} ion in the so-called "cysteine" binding site.

 Published on Web 06/08/2010

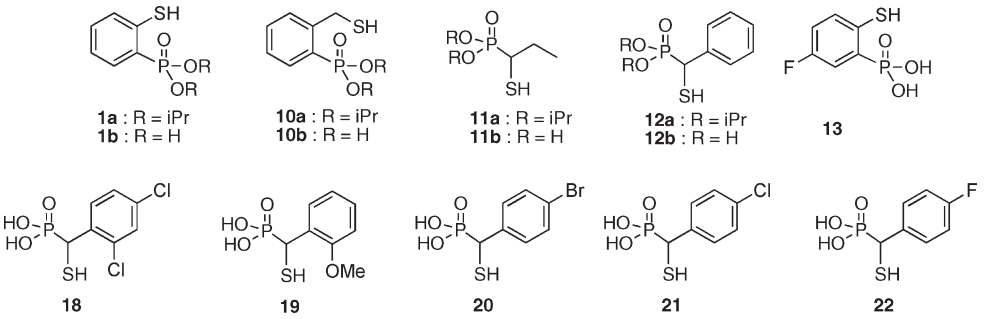

Figure 1. Mercaptophosphonates synthesized as potential MBL inhibitors.

Scheme 1

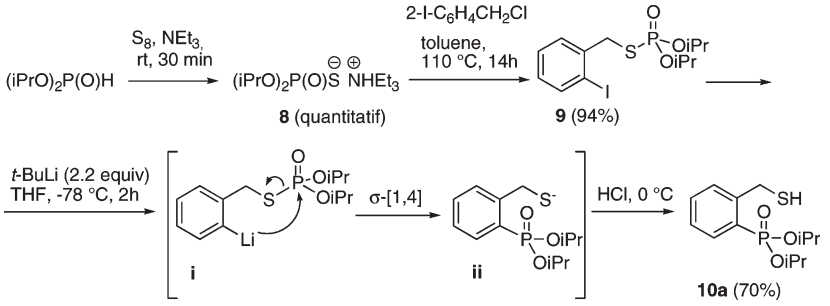

In the paper, we investigate the inhibitory effect of 14 mercaptophosphonate derivatives (Figure 1: **1a**,**b**; **10**−**12a**,**b**; **13**; **18**−**22**) belonging to three structural families (α-mercaptophosphonates, 2-sulfanyl benzenephosphonates, and 2-(sulfanylmethyl)phenylphosphonates) against a representative of the three subclasses of MBLs (VIM-4 (B1),[19] CphA (B2),[20] and L1 (B3)[21]). VIM-4 belongs to the subclass B1 acquired enzymes such as SPMs,[22] SIMs,[23] GIMs,[24] and IMPs.[25] The VIM-type enzymes are clinically relevant, and they have caused important outbreaks.[26−31] Because they are well characterized enzymes, CphA and L1 or FEZ-1[32] enzymes were used as models for their subclasses.

Crystallographic studies were conducted on the enzyme (CphA, VIM-4, FEZ-1)−inhibitor (**10a** and **18**) complexes. Both complexes were solved for CphA. Unfortunately, no complex with the two other MBLs was obtained. Consequently, molecular modeling of the complexes allowed different binding modes of the inhibitor in complex with examples from the MBL subclasses to be proposed.

Results

The selected mercaptophosphonates (including phosphonic esters and their corresponding acids) belong to three structural families (α-mercaptophosphonates, 2-sulfanyl benzenephosphonates, and 2-(sulfanylmethyl)phenylphosphonates), depending on the relative positions of the two phosphorus and sulfur functions in their structures. On the basis of the promising results obtained in several studies with thiomandelic acid, its phosphonic analogue **12b** was first chosen as a representative structure of the α-mercaptophosphonate family. Then compounds **1b** and **10b**, belonging to 2-sulfanyl benzenephosphonates and 2-(sulfanylmethyl)phenylphosphonates, respectively, have been selected for the study. For a structure−activity relationship (SAR) study, structural modifications on these three types of mercaptophosphonic acids have been envisaged. The structures of compounds **1** and **10** are not easy to modify by the synthetic procedure described in this paper (only one derivative of **1b** was synthesized, the fluorinated compound **13**). However, the procedure used for **12b** enabled us to prepare other α-mercaptophosphonates (i.e., aliphatic **11** and aromatic **18**−**22** derivatives). Derivatives bearing halogen atoms on the aromatic ring have been particularly targeted (**18**, **20**−**22**), as it is now well established that halogen bond interactions could play an important role in molecular recognition processes.[33]

Synthesis of Inhibitors 10a and 18. Compound **10a** was synthesized in three steps,[34] starting from commercially available diisopropyl phosphite (Scheme 1). Thiophosphate ammonium salt **8** was obtained quantitatively by reacting diisopropyl phosphite with elemental sulfur (S_8) in the presence of triethylamine. Then, S-alkylation of **1** with 2-iodobenzyl chloride in refluxing toluene led to thiophosphate **9** in 94% yield. A [1,4]-sigmatropic rearrangement was used to transform thiophosphate **9** into the 2-(sulfanylmethyl)phenylphosphonate **10a**. The iodide−lithium exchange by reacting **9** with *tert*-butyllithium led to carbanion **i**, which rearranged into sulfanyl **ii** via the migration of the phosphoryl group from the sulfur atom on the carbon aromatic ring. At the end of the reaction, the acidic hydrolysis of the sulfanyl led to the desired compound **10a**. The overall yield of the three steps was 66%.

Compound **18** was synthesized in five steps, as shown in Scheme 2. First, α-hydroxyphosphonate **14** was prepared by condensation of 2,4-dichlorobenzaldehyde with diisopropyl phosphite. Alcohol **14** was then transformed in three steps into the corresponding thiol **17** using a sequence described previously by some of us:[35] transformation of **14** into its *p*-nitrobenzenesulfonate derivative **15**, nucleophilic substitution using potassium thiocyanate leading to thiocyanatomethylphosphonate **17**, and reduction of the thiocyanate function with sodium borohydride to afford, after acidic hydrolysis, the expected α-sulfanylphosphonate **17**. Compounds **14**, **15**, and **16** have been used without purification in the next step (their purity was >95% by NMR spectroscopy). Only α-sulfanylphosphonate **17** was purified by flash chromatography before its transformation into phosphonic

Scheme 2

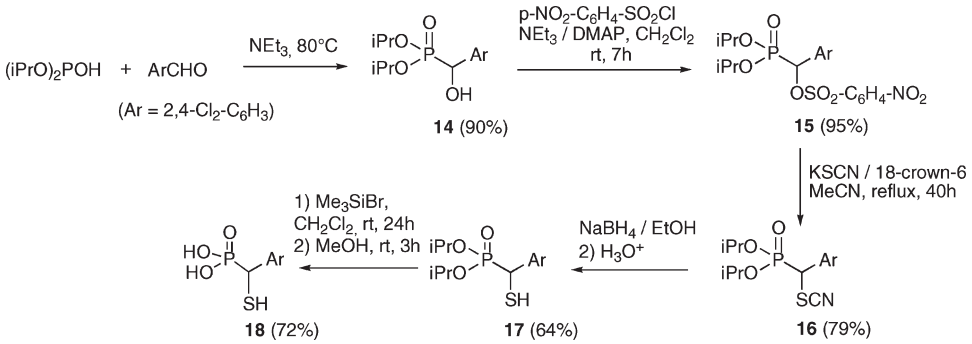

acid **18** by treatment with Me_3SiBr followed by methanolysis.[36] The overall yield of the five steps was 31%.

Synthesis of the 12 Other Inhibitors. The *o*-mercaptobenzenephosphonate **1a**, its phosphonic acid derivative **1b**, and the fluorinated derivative **13**, as well as the α-mercaptophosphonates **11a** and **12a**, were synthesized as described previously.[35,37,38] The phosphonic acids **10b**, **11b**, and **12b** were obtained from their phosphonic esters **10a**, **11a**, and **12a** by the same procedure used to transform ester **17** into its acid **18**. The α-mercaptophosphonic acids **19**, **20**, **21**, and **22** were prepared from diisopropyl phosphite and the corresponding aromatic aldehyde, in five steps, by the same method used for the synthesis of compound **18**.

Screening of the Inhibitory Activities of Mercaptophosphonates on MBLs. The screening for inhibition against the subclass B1 VIM-4, the subclass B2 CphA, and the subclass B3 L1 enzymes was investigated with the first set of four mercaptophosphonates, each of them in both ester and acid forms (**a** and **b**, respectively): the *o*-mercaptobenzenephosphonate **1**, the *o*-phosphonylated benzylic thiol **10**, and two α-mercaptophosphonates, one aliphatic **11** and one aromatic **12** (Figure 1). The determined inhibition constants (K_i) are shown in Table 2. When K_i values were higher than 20 μM, the compounds were not considered as good inhibitors and accurate K_i values were not determined. The *o*-mercapto(phenylphosphonic) acid **1b** is already known as a tight-binding inhibitor of the bovine intestinal alkaline phosphatase (K_i = 0.21 μM) and of the *Escherichia coli* alkaline phosphatase (IC_{50} < 10 μM).[17] In this study, while this compound is an efficient competitive inhibitor of the three subclasses of MBLs with K_i values ranging from 2 to 12 μM, its ester counterpart (**1a**) had no inhibitory effect on the tested enzymes. Compound **10b** seems to behave as a strong chelator, since the residual activities of VIM-4 and L1 are considerably increased upon the addition of an excess of $ZnCl_2$ (50 μM) in the buffer. The inactivation observed in the absence of added Zn^{2+} could be explained by the chelation of the Zn^{2+} ion by **10b**. With the exception of the inhibition of CphA, **11a** shows no significant inhibitory activity against any of the other MBLs tested. Its acid counterpart (**11b**) inhibits CphA as well as VIM-4 with K_i values of ~10 μM. The other three compounds **10a**, **12a** and **12b** behaved as good inhibitors for the three MBLs with K_i values ranging from 0.25 to 32 μM. **10a** also inhibited the N220G-N116H extended-spectrum mutant of CphA (the K_i value was 7 μM). We hoped that compounds **13** and **18**−**22** bearing various substituents on the aromatic ring would provide better inhibitory effect than their unsubstituted counterparts **1b** and **12b**, respectively. The study of these compounds also allowed us to examine the importance of the nature or the position of the substituent on the aromatic ring in the inhibition. Interestingly, the inhibition of CphA is reduced when a fluorine atom is added at position C_5 of the aromatic ring (Table 2, **1a** vs **13**). In contrast, the inhibition of VIM-4 and L1 remains similar to that of the original compound with K_i values of 2 and 4 μM, respectively. A comparison of **12b** to its substituted derivatives highlighted the most interesting results obtained with the dichlorinated derivative **18**. The presence of the two chlorine atoms on the aromatic ring (in C2 and C4) has enhanced the inhibition for all three enzymes with a clear improvement for the L1 enzyme. Compound **19** inhibits the VIM-4 enzyme similarly to **18** (with a K_i of 2 and 1 μM, respectively); however, for the CphA and L1 enzymes, its propensity of inhibition is decreased (Table 2). As compound **19** contains an OCH_3 function at C_2 position, the difference in inhibition could be due either to the loss of the chlorine group at C_4 or to the different nature of the group at C_2. Compounds **20**, **21**, and **22** are functionalized at the same position (C_4), and that results in a lower inhibition of VIM-4 compared to **18**; thus, the substituent on C_4 does not seem important, whereas position C_2 seems relevant for the VIM-4 inhibition. Mercaptophosphonic acids **19**, **20**, **21**, and **22** are not as efficient as **18** in the inhibition of MBLs subclasses. They exhibit specific profiles of inhibition: **19** is directed toward VIM-4,; **20** and **21** are directed toward L1; **22** is directed toward CphA.

In order to determine the interaction mediating the positioning of the inhibitors in the active site of each enzyme, crystallographic and docking studies were performed with **10a** and **18**, the two inhibitors active against the three subclasses.

Crystallographic Studies. CphA (B2). To elucidate the molecular basis of the inhibition of CphA, the crystal structure of the two inhibitor (**10a** and **18**)/CphA mutant N220G complexes were solved. The N220G mutant was used instead of the wild-type CphA enzyme because this mutant crystallizes much more easily and rapidly than the wild-type enzyme.[39,40] The mutation of this noncatalytically essential Asn residue in Gly does not modify the kinetic parameters of the enzyme[41] or the three-dimensional structure.[39,40] The K_i values obtained for the **10a** and **18** compounds and the N220G CphA enzyme were 6 and 3 μM, respectively. Therefore, crystals of N220G CphA were soaked in the presence of the inhibitors. The crystal structures were solved by molecular replacement using the wild-type structure of CphA (PDB code 1X8G) as model. After refinement, almost all residues lay in the allowed or favored region in the Ramachandran plot. Stereochemical parameters were calculated by PROCHECK and WHAT_CHECK and were in the range expected for structures with similar resolutions. The

Table 1. X-ray Data Collection and Structure Refinement for CphA−**10a** and CphA−**18**

	CphA−**10a**	CphA−**18**
Data Collection Statistics		
wavelength [Å]	1.5418	1.5418
cell parameter [Å]	$C222_1$	$C222_1$
a, b, c [Å]	42.65, 100.66, 1116.99	42.73, 100.88, 117.56
α, β, γ [deg]	90, 90, 90	90, 90, 90
molecules/ asymmetric unit	1	1
resolution [Å]	19.59−1.44	19.65−1.41
R_{sym}	0.041/0.112	0.042/0.084
no. unique reflexes	43889/3054	45999/3175
completeness [%]	99.72/96.30	98.33/92.92
multiplicity	11.6/6.6	9.8/6.3
$I/\sigma(I)$	40.7/16.3	37.3/16.6
R_{work}	0.1225/0.123	0.1434/0.146
R_{free}	0.1408/0.153	0.1545/0.176
Root Mean Square Deviation from Ideal		
bonds [Å]	0.011	0.011
angles [deg]	1.565	1.510
proteins atoms	1919	1889
Zn^{2+}	1	1
water	290	285

Table 2. Competitive Inhibition Constant K_i (μM) of the Different Mercaptophosphonate Compounds for One Member of Each MBL Subclass[a]

	VIM-4 (B1)		CphA (B2)	L1 (B3)	
compd	Zn^{2+}	no Zn^{2+}	no Zn^{2+}	Zn^{2+}	no Zn^{2+}
1a	> 250	> 250	> 250	> 250	> 250
1b	4	2	7	12	9
10a	12	3	2	14	3
10b	> 400	1	0.5	> 50	2
11a	> 20	> 20	2	> 40	> 40
11b	6	11	15	> 40	> 80
12a	8	3	0.25	16	20
12b	3	2.5	11	32	> 100
13	13	2.5	> 40	4	40
18	4	1	5	0.40	0.40
19	4	2	15	4	9
20	13.5	5.5	13	1.7	8.4
21	10	6.7	24	0.7	3.8
22	11	16	1	18	> 20

[a] SD values are below 10%. ND: not determined. Zn^{2+}: the added Zn^{2+} concentration is 50 μM. No Zn^{2+}: no added Zn^{2+}; the Zn^{2+} concentration is below 0.4 μM.

crystallographic and model statistics for both structures are summarized in Table 1.

Structure of the CphA−10a Complex. To investigate the structural basis of the inhibition of CphA by the diisopropyl [2-(sulfanylmethyl)phenyl]phosphonate (**10a**), crystals of the inhibitor associated with the CphA enzyme were produced. The structure was refined in a resolution range of 19.6 to 1.44 Å. The refinement yielded an R_{work} of 0.1228 and R_{free} of 0.1415. The refined CphA−**10a** complex structure comprises all 227 protein residues. The N-terminus, C-terminus, and some surface oriented residues exhibit high mobility (expressed by high *B*-values). Furthermore, 1 Zn^{2+} ion, 10 sulfate ions, 1 molecule of **10a**, 3 glycerol molecules, and 290 water molecules (Table 1) were identified in the electron density. In the active site, the electron density corresponds to the shape of the inhibitor (Figure 2a). The positions of the sulfur and phosphorus atoms of the inhibitor molecule could be established by calculating an anomalous map. As in the native structure, the Ala195 residue is in a disallowed region of the Ramachandran plot. Ala195 ($\psi = 105°$, $\phi = 156°$) is located on a loop between two strands, which belongs to the active site and comprises the functionally important His196 residue.

The protein structure of CphA in the complex is very close to that of the native protein (PDB code 1X8G), with a root-mean-square deviation between the Cα atoms of 0.307 Å. Superimposition of the two structures shows that the binding of the inhibitor leads to a movement of the Gly232-Asn233 loop located at the active site entrance so that it encloses the active site (Figure 2b).

The structure of the CphA−**10a** complex shows that the **10a** inhibitor binds to the catalytic Zn^{2+} and interacts with the enzyme active site with both electrostatic and hydrophobic contacts. As previously proposed for thiomandelic acid in the subclass B1 BcII enzyme,[8,42] the inhibitor **10a** binds the Zn^{2+} ion of CphA via its sulfur (Figure 2b). Typically in CphA structures, the Zn^{2+} ion is coordinated to the three MBL conserved Cys221, Asp120, and His263 residues and an ion from the buffer solution (e.g., a carbonate ion in 1X8G). Here, the sulfur of the inhibitor completes the tetrahedral coordination sphere of the Zn^{2+} ion. The distance between the Zn^{2+} ion and the sulfur of the inhibitor is 2.31 Å. Moreover, two water molecules are at distances of 3.20 (W333) and 3.11 Å (W435) from the sulfur atom. Both water molecules are involved in a large hydrogen bond network within the protein. W333 is situated 2.85 Å away from the conserved Lys224 residue and is also in contact (2.99 Å) with the backbone nitrogen of Asn233. W435 has additional contacts to Asn233 ND2 (2.79 Å), to His196 NE2 (2.93 Å), and also to O21 of the phosphonato group (3.08 Å) (Figure 2b). His196 NE2 and His263 NE2 are also at distances of 3.50 and 3.42 Å from the sulfur atom of the inhibitor.

There is an interaction between the O1 of the phosphonato group and CE2 of the Phe156 residue (2.89 Å). The methyl groups of the inhibitor molecule are involved in several interactions with the protein, notably C91 with Val67 CG2 (3.19 Å), C91 with Leu161 CD1 (3.38 Å), C101 with Leu161 CD1 (3.68 Å), C101 with Thr157 O (3.30 Å), C92 with Ile153 CD1 (2.92 Å), C92 with Thr157 OG1 (3.47 Å), C102 with Asp120 OD1 (3.24 Å), and C102 with Thr119 OG1 (3.32 Å). A hydrophobic contact is observed between Cβ from Asn233 and the aromatic ring of compound **10a**. The Cβ atom is 3.8 Å from the center point of the ring structure (Figure 2c).

Structure of the CphA−18 Complex. To investigate the structural basis of the inhibition of CphA by the [(2,4-dichlorophenyl)(sulfanyl)(methyl)]phosphonic acid (**18**), crystals of the complex of CphA with the inhibitor were produced. The structure was refined in the range of 19.65−1.41 Å to R_{work} = 0.1435 and R_{free} = 0.1548. The CphA−**18** complex structure contains all 227 protein residues. The first two N-terminal residues are refined in two orientations. The last C-terminal residue is half occupied only. Moreover, some side chains show high mobility and are disordered or not fully occupied. One Zn^{2+} ion, 5 sulfate ions, 1 molecule of **18** (Figure 3a), 2 glycerol, and 285 water molecules (Table 1) are found in the structure. The orientation of the **18** molecule could be verified by calculation of the anomalous map. Some unexplained density remains in the active site; however, this supplementary electron density could not be attributed to water molecules or to an additional inhibitor molecule. The protein structure of CphA in the complex is very close to that of the native protein (1X8G), with a root-mean-square deviation between the Cα atoms of

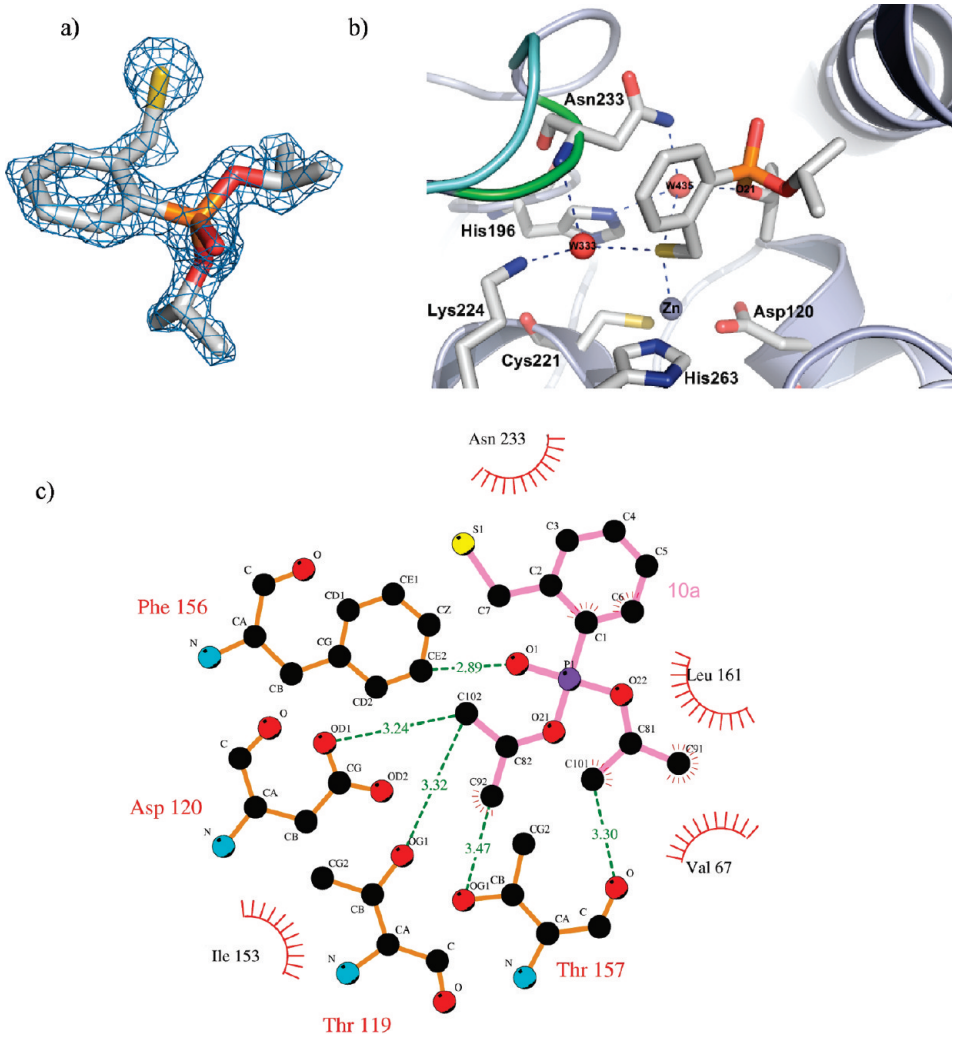

Figure 2. Crystallographic structure of the CphA−**10a** complex. (a) $2F_o - F_c$ map at 1σ level. The electron density in the active site of CphA corresponds to the shape of molecule **10a**. (b) Inhibitor **10a** interacts with the Zn^{2+} ion via its sulfanyl group. Water molecules (W) and Zn^{2+} ion are represented as red and gray spheres, respectively. The "closed" position of the Gly232-Asn233 loop in the complex is represented in green to emphasize the modification compared to the native structure (in cyan). (c) Interactions between CphA and the phosphonato and methyl groups of **10a** depicted using LIGPLOT.[66] The hydrophobic interaction between the Asn233 residue and the aromatic ring of **10a** is also represented. In the schematic drawing, hydrogen bonds are shown as dashed green lines. Ligand and protein hydrophobic contacts are represented as curved red combs.

0.267 Å. The difference with the **10a** complex structure is 0.171 Å. Once more, the binding of the inhibitor leads to the "closed" position of the Gly232-Asn233 loop located at the active site entrance. Surprisingly, in contrast to the CphA−**10a** complex, the Zn^{2+} ion is bound by the phosphonato oxygen atoms O11 (1.98 Å) and O12 (3.38 Å) of the inhibitor **18** and not by the sulfur (Figure 3b) (it is worth noting that in **10a** the phosphorus function is a phosphonic ester while in **18** it is a phosphonic acid). Furthermore, O11 is in contact with water molecule 419 at a distance of 2.57 Å. The O12 of the phosphonato group also interacts with the NE2 of the His263 residue (3.38 Å). The same oxygen is close to the NZ of the Lys224 residue (2.72 Å), and the third oxygen O13 of the phosphonato group lies in the vicinity of the NE2 of the His196 residue (2.76 Å). The water molecule 473 (W473) stabilizes the side chain of Asn233 through a contact to ND2 (2.77 Å). Moreover, W473 is in contact with the O13 of the phosphonato group (2.88 Å) and with His196 NE2 (3.19 Å). The sulfur of the inhibitor is in contact with a water molecule (W347, 3.06 Å) and the backbone nitrogen of the Asn233 residue (3.45 Å). This latter interaction stabilizes the "closed" form of the Gly232-Asn233 loop. The Cl1 chlorine atom is also in contact with the CE1 carbon of the His263 residue (3.35 Å), while the second chlorine atom Cl2 binds a water molecule (W284, 3.57 Å).

Modeling Studies. Crystals of the VIM-4 (B1) and FEZ-1 (B3) enzymes were obtained as described previously[43,44] and soaked with **10a** and **18**. Unfortunately, no electron density corresponding to the inhibitors was observed in the active sites of the solved structures. Therefore, modeling studies were performed with VIM-4 (B1), CphA (B2), and the monomeric FEZ-1 enzyme. This study is much easier than with L1 (B3), as the latter enzyme is a homotetramer.[45] In the following, Zn1 refers to the Zn^{2+} ion in the so-called "histidine" binding site where it is coordinated by three conserved histidine residues (His116-His118-His196) while Zn2 corresponds to that in the "cysteine" binding site (Asp120-Cys221-His263 in the B1 enzyme and Asp120-His121-His263 in the B3 enzyme). In CphA, the sole Zn^{2+} ion binds in the "cysteine" site (Asp120-Cys221-His263).

VIM-4−18. Manual docking of compound **18** in the active site of VIM-4 was the starting point of this study, followed by three steps of energy minimization. Dynamic simulation and

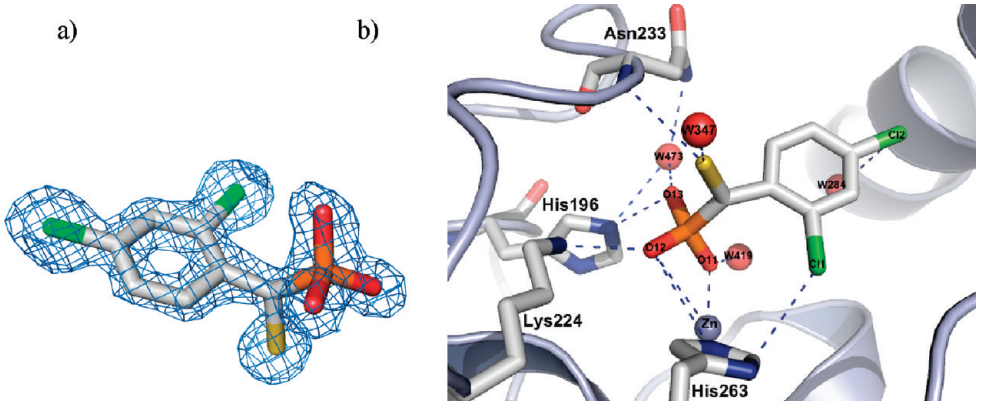

Figure 3. Crystallographic structure of the CphA−**18** complex. (a) $2F_o - F_c$ map at 1σ level. The electron density in the active site of CphA reflects the shape of molecule **18**. (b) Inhibitor **18** interacts with the Zn^{2+} ion via two oxygen atoms of the phosphonato group. Water molecules (W) and Zn^{2+} ion are represented as red and gray spheres, respectively.

Table 3. Characterization of the Potential Binding Modes between VIM-4 and **18** and **10a**[a]

		18 conformation						**10a** conformation	
parameter		1	2	3	4	5		1	2
energy (kcal/mol)									
interaction energy		−144.4	−141.85	−144.47	−123.65	−81.93		−210.61	−95.2
distortion energy of **18**		21.53	22.75	26.04	21.33	2.08		22.45	5.84
distance of interaction (Å)									
Zn1	His116	2.23	2.52	2.14	2.10	2.16		(6.24)	(4.47)
	His118	2.12	2.16	2.09	2.16	2.13		2.21	2.16
	His196	2.10	2.13	2.10	2.22	2.10		2.19	2.27
	18-S					2.45	**10a**-S	2.48	2.36
	18-O_{11}	2.09		2.05			**10a**-O_1	1.86	
	18-O_{13}		1.89	1.94			Asp120		1.92
	Cys221	2.23	2.25		2.21				
Zn1−Zn2		3.73	4.20	5.28	4.16	3.93		5.74	4.35
Zn2	Asp120-O_1	1.96	2.00	1.91	1.97	1.92		1.97	1.91
	Asp120-O_2	1.98	2.01		2.02	2.27		1.98	
	Cys221	2.18	2.16	2.11	2.17	2.10		2.13	2.12
	His263	(3.76)	2.13	2.09	2.15	2.10		2.09	2.21
	18-O_{13}	1.89			2.15		His116		2.15

[a] Distances in parentheses are too long for the residue to be a Zn^{2+} ligand. The interaction energy is the difference between the energy of the complex and the energies of its constituents in the complex geometry. The distortion energy is the sum of the distortion energies of the constituents, i.e., the difference between the energy of the constituents in the complex geometry and the energy of their optimized geometries.

energy minimization were successively employed to obtain optimal conformations of the complexes. Thus, eight different conformations representing four different binding modes were obtained (Table 3). Among them, only one (conformation 5) was mediated by the sulfanyl group of compound **18**, with the smallest interacting energy (−82 kcal/mol). The other three, with a fifth conformation (conformation 4) obtained after minimization of the VIM-4−**18** complex built from the crystallographic complex CphA−**18**, were characterized by interactions between Zn^{2+} ions and the phosphonato group. Conformation 1 exhibited a coordination between one oxygen (O11) of the phosphonato group with Zn1 and a second interaction between a second phosphonate oxygen (O13) and Zn2. Conformation 2 was characterized by a Zn1−O13 bond, whereas conformation 4 had a Zn2−O13 interaction. Finally, conformation 3 had two of its oxygens (O11 and O13) coordinating Zn1. Apart from conformation 4 presenting a small interacting value, the other three conformations (1, 2, 3) were characterized by a strong interaction energy value of −144 kcal/mol with a similar deformation of compound **18**, corresponding to the likely model of binding. This possible binding mode between VIM-4 and **18** would occur via a binding of the inhibitor phosphonato group with Zn1 or both Zn^{2+} ions in the active site (Figure 4a). Interestingly, all our models were highly variable. Indeed, as highlighted in Table 3, the positions of the Zn^{2+} ions, particularly Zn2, and the distance between them were strongly perturbed because of some rearrangement of the overall fold of the protein. This mobility is emphasized by the change in the coordination spheres of both Zn^{2+} ions, and in conformations 1, 2, and 4, Cys221 was now interacting with both of them via a rotation of its position. Furthermore for conformations 1 and 2, Asp120 was binding to Zn2 via two oxygen atoms and not one as usually described. Thus, out of the three conformations, conformation 3 seems the most probable mode of binding, as the coordination sphere of the Zn^{2+} ions is not perturbed (Figure 4a). This model of interaction is coherent with the crystallographic model of CphA−**18**.

VIM-4−10a. As for inhibitor **18**, several complex models were built by manual docking or by using the conformation of compound **10a** from the crystallographic CphA−**10a** complex. After minimization conducted as previously, two conformations were selected corresponding to two different binding modes both mediated by the inhibitor sulfanyl group interacting with Zn1 (Table 3). Conformation 1 presented

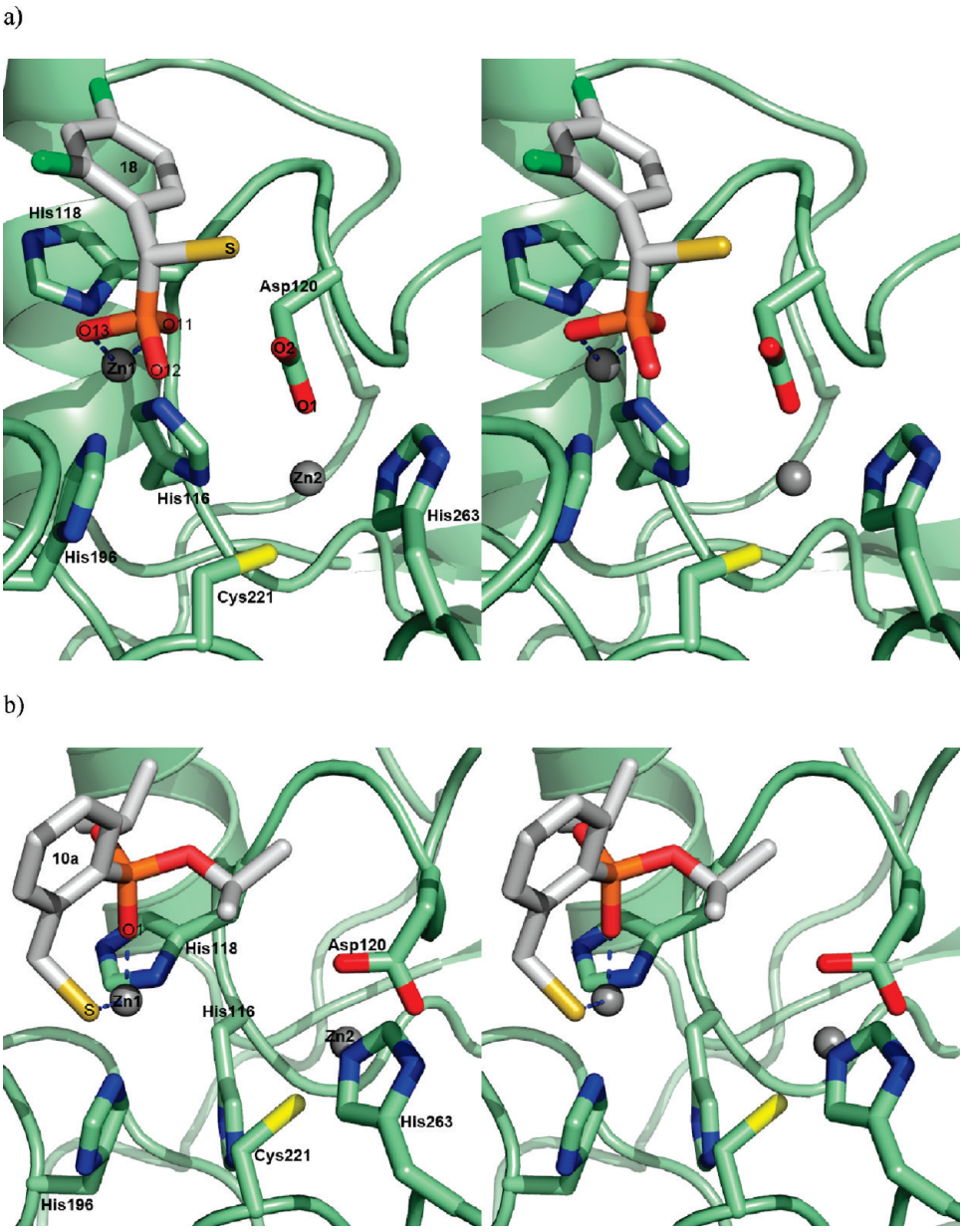

Figure 4. Molecular modeling of VIM-4: stereoviews of all conformations. (a) Conformations with the best interactions representing the possible mode of binding of compound **18** to VIM-4. The inhibitor interacts with Zn1 via two oxygen atoms (O11 and O13) of its phosphonato group. (b) Conformation representing the possible binding mode of compound **10a** to VIM-4. The inhibitor interacts with Zn1 via one oxygen atom (O1) of its phosphonato group and via its sulfanyl group.

two interactions between **10a** and VIM-4, one S−Zn1 and one O11−Zn1; this conformation presented a stronger interaction than conformation 2 characterized by the sole sulfanyl−Zn1 coordination (Figure 4b). As for the crystallographic complex CphA−**10a**, an interaction via the sulfanyl group was preferred to an interaction occurring via the phosphonato group of **10a**, and this binding mode seems to be the most probable.

CphA−18. The optimization of the crystallographic complex CphA−**18** and other manually built complexes was performed as previously. Three different binding modes were considered (Table 4). Interestingly, in the first model corresponding to the optimization of the crystallographic complex, the binding of **18** with the protein evolved from two interactions between the Zn^{2+} ion and two oxygen atoms (O11 and O12) of the phosphonate to one interaction via its sulfanyl group to the Zn^{2+} ion. In the second, it is one oxygen atom (O11) of the phosphonato group that coordinates the Zn^{2+} ion. Finally, in the third conformation, two oxygen atoms (O11 and O12) of the phosphonato group are binding to the metal. This last interaction is the one resulting in the best interaction energy (Figure 5c). This interaction is similar to the observed crystallography results; however, the rmsd value of 0.791 Å emphasizes that if the interaction remains the same, the overall fold of the protein is significantly different. This result is consistent with an interaction taking place between the phosphonato group and the Zn^{2+} ion rather than the sulfanyl group.

CphA−10a. The optimization was performed on various manually docked complexes and on the crystallographic CphA−**10a** complex. Different models were obtained, representing one major binding mode, since all of them occurred

Table 4. Characterization of the Potential Binding Modes between CphA and **18** and **10a**[a]

		18 conformation					**10a** conformation			
parameter		1	2	3	structure		1	2	3	structure
energy (kcal/mol)										
interaction energy		−87.3	−52.67	−91.3			−114.69	−144.45	−62.35	
distortion energy of **10a**		3.56	1.84	17.66			6.9	14.67	10.54	
distance of interaction (Å)										
Zn	Asp120-O_1	1.97	1.93	1.98	1.95		2.00	2.12	1.89	1.96
	Asp120-O_2						2.02	2.01		
	Cys221	2.14	2.18	2.24	2.32		2.19	2.17	2.15	2.34
	His263	2.14	(4.20)	2.2.1	2.08		2.20	(6.04)	2.14	2.11
	18-S	2.34				**10a**-S	2.31		2.28	2.30
	18-O_{11}		1.96	2.11	1.99	**10a**-O_1		1.88		
	18-O_{12}			2.03	3.38	His118		2.20		

[a] Conformations 1 (compound **18**) and 3 (compound **10a**) are the results of the minimization of the X-ray structure of both complexes. Interaction distances of the crystallographic structure of both complexes are represented in this table. Distances in parentheses are too long for the residue to be a Zn^{2+} ligand. The interaction energy is the difference between the energy of the complex and the energies of its constituents in the complex geometry. The distortion energy is the sum of the distortion energies of the constituents, i.e., the difference between the energy of the constituents in the complex geometry and the energy of their optimized geometries.

via the sulfanyl counterpart of compound **10a** with the exception of conformation 2 that binds the Zn^{2+} ion via the oxygen (O1) of the phosphoryl (P═O) group (Table 4). This latter conformation exhibits a much stabilized complex, as its energy of interaction is −144 kcal/mol with a meaningful deformation of the compound (Figure 5b). The root mean square deviation of model 3 to the original structure has been calculated (0.915 Å) and has revealed an important change to the overall fold of the protein. This deviation is even higher in the case of conformation 2 with a value of 1.728 Å making evident the important changes to the overall structure. In this case, the minimization process yielded many results consistent with the crystallography results (Figure 5a); however, the preferred conformation, which is significantly different to the initial protein, occurs with a different binding mode when compared to the crystallography results.

FEZ-1−18. Many conformations were obtained for this complex; however, all the interactions were characterized by O12−Zn1 and O11−Zn2 binding (Figure 6a), with an energy of −144 kcal/mol as the best interaction energy (Table 5). The coordination spheres of both Zn^{2+} ions were not conserved in those conformations, as His116 and His121 were now too far from the Zn^{2+} ions to coordinate them. This distortion of the protein was possibly due to the chosen charge of 1.5 for the Zn^{2+}. As a matter of fact, the net charge of the Zn^{2+} ions was determined at the quantum chemistry level for a complex involving the inhibitor and two Zn^{2+} ions. However, in the case of the FEZ-1−**18** complex, the most favorable interaction occurs via the phosphonato group, as described for VIM-4 and CphA.

FEZ-1−10a. Four conformations were obtained at the end of FEZ-1−**10a** optimization, with two different binding modes (Table 5). Both of them were characterized by the binding of the sulfanyl group to the protein, with an interaction with Zn1 for the first conformation and the second one occurring between its sulfanyl and Zn2 and the oxygen (O1) of the phosphonato group and Zn1. This latter conformation, conformation 2 (Figure 6b), exhibited a strong interaction (−243 kcal/mol) that represented the strongest interaction of all obtained models. Therefore, conformation 2 is the most probable mode of interaction between FEZ-1 and **10a**. The interaction between the sulfanyl group and the Zn^{2+} cation is consistent with the crystallographic data; however, the additional interaction via the phosphonato group highlights the complex interactions of this compound. Once again, all conformations had Zn^{2+} coordination different from the usual ones as His116 or His121 and/or His263 was too far from the Zn^{2+} ions to interact.

Discussion

To date, in contrast to active serine β-lactamases, no clinically useful inhibitor of MBLs is available despite the huge number of tested molecules. The development of a broad spectrum MBL inhibitor is challenging because of the structural diversity and differences in metal utilization by these enzymes.[5] Many already described MBL inhibitors as "potent" inhibitors active only against one subclass of MBLs or even only against one specific enzyme,[7,46−49] rather than as "good" inhibitors active against the three subclasses. However, recently, Liénard et al. reported the most potent broad spectrum inhibitor ever described that exhibits K_i values lower than 1 μM for all tested MBLs (BcII, IMP-1, CphA, L1, and FEZ-1).[11] This compound, as well as the thiomandelic acid[8] or D-captopril,[10] combines in its structure a thiol, a carboxylate, and an aromatic ring. Thiol, phosphonic acid, and carboxylate groups have an affinity for metal ions. Hence, their phosphorus analogues, i.e., mercaptophosphonic acids and their ester counterparts, were synthesized and investigated as broad spectrum MBL inhibitors. Compound **12b** is the phosphonate analogue of the well described thiomandelic acid.[8] Among the 14 tested compounds, **1b**, **10a**, **12a**, and **12b** behaved as good inhibitors for the three subclasses of enzymes with K_i values ranging from 0.25 to 32 μM. The strategy used for enhancing the inhibitory potency of phosphonic acids against metallophosphatases has been to substitute one carbon with a halogen;[17,18] the same strategy has also been employed in this study. Here, compound **18**, which differs from compound **12b** by the presence of two chlorine atoms on the phenyl ring, showed an increased inhibition for all the three representative enzymes with a clear improvement for the subclass B3 L1 enzyme. The K_i values were 1, 5, and 0.4 μM for the B1, B2, and B3 enzymes, respectively. Thus, the K_i values are in the same range as those observed for Lienard's compound[11] with the exception of the value obtained for the subclass B2 enzyme which is slightly higher for **18**. However, **18** is much better than the thiomandelic acid as a subclass B2 inhibitor[8] and in contrast to the latter thus presents a broad inhibitory spectrum.

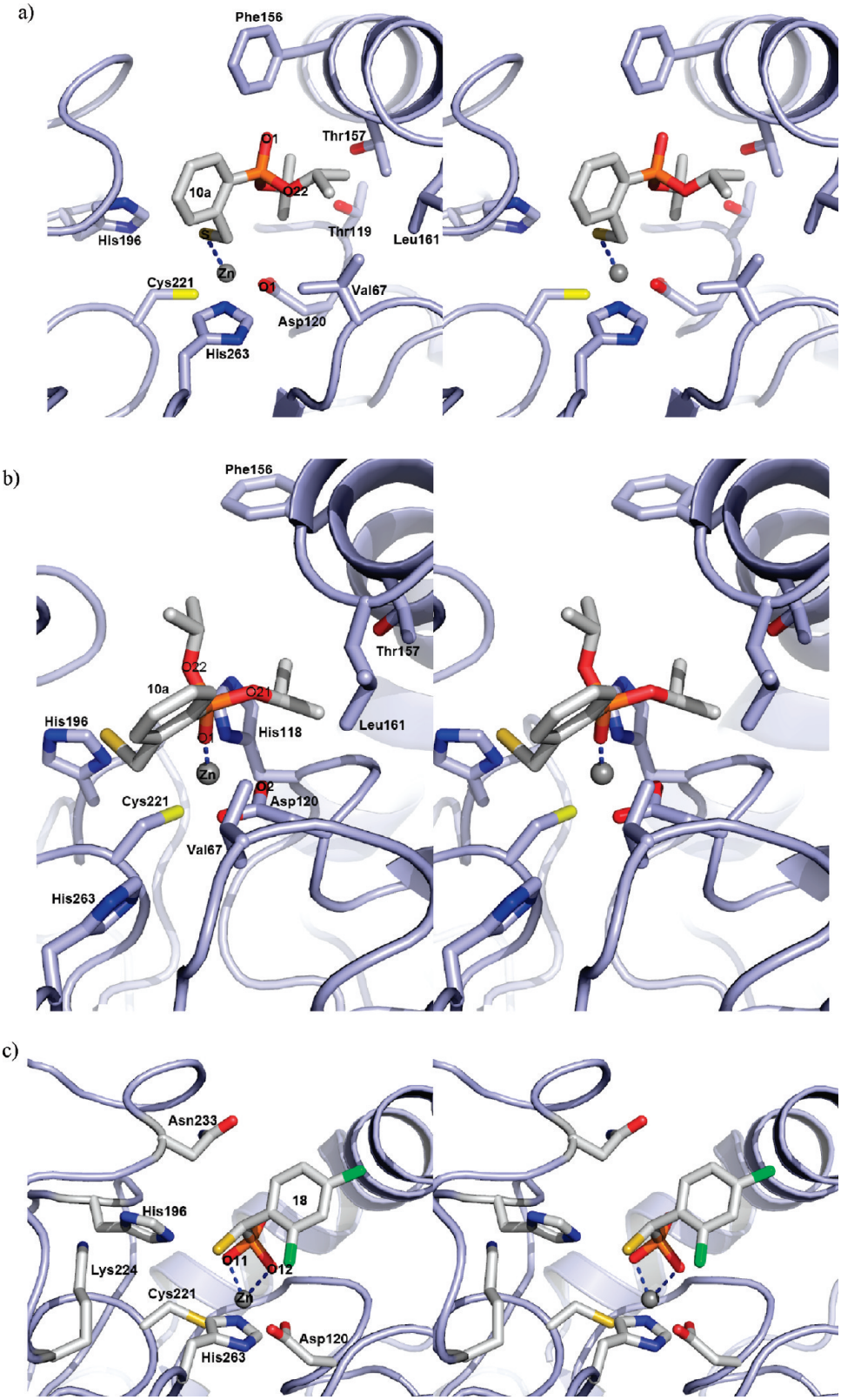

Figure 5. Molecular modeling of CphA: stereoviews of all conformations. (a) CphA−**10a**: The inhibitor interacts with the Zn^{2+} ion via its sulfanyl group. This conformation (3) is similar to the crystallography data but is not that exhibiting the best interaction energy. (b) CphA−**10a**: The inhibitor interacts with the Zn^{2+} ion via one oxygen atom (O1) of the phosphonato group. This conformation represents the best computed interaction between **10a** and CphA. (c) CphA−**18**: The inhibitor interacts with the Zn^{2+} ion via two oxygen atoms (O11 and O12) of the phosphonato group. This conformation is in agreement with the crystallographic data.

To explore the enzyme−inhibitor interactions, compounds **10a** and **18** were chosen to obtain the crystallographic structures of the complexes. We succeeded in obtaining the structures of the CphA−**10a** and CphA−**18** complexes. Both inhibitor enzyme complexes are stabilized by a network of hydrophobic contacts and hydrogen bonds. Interestingly, these complexes

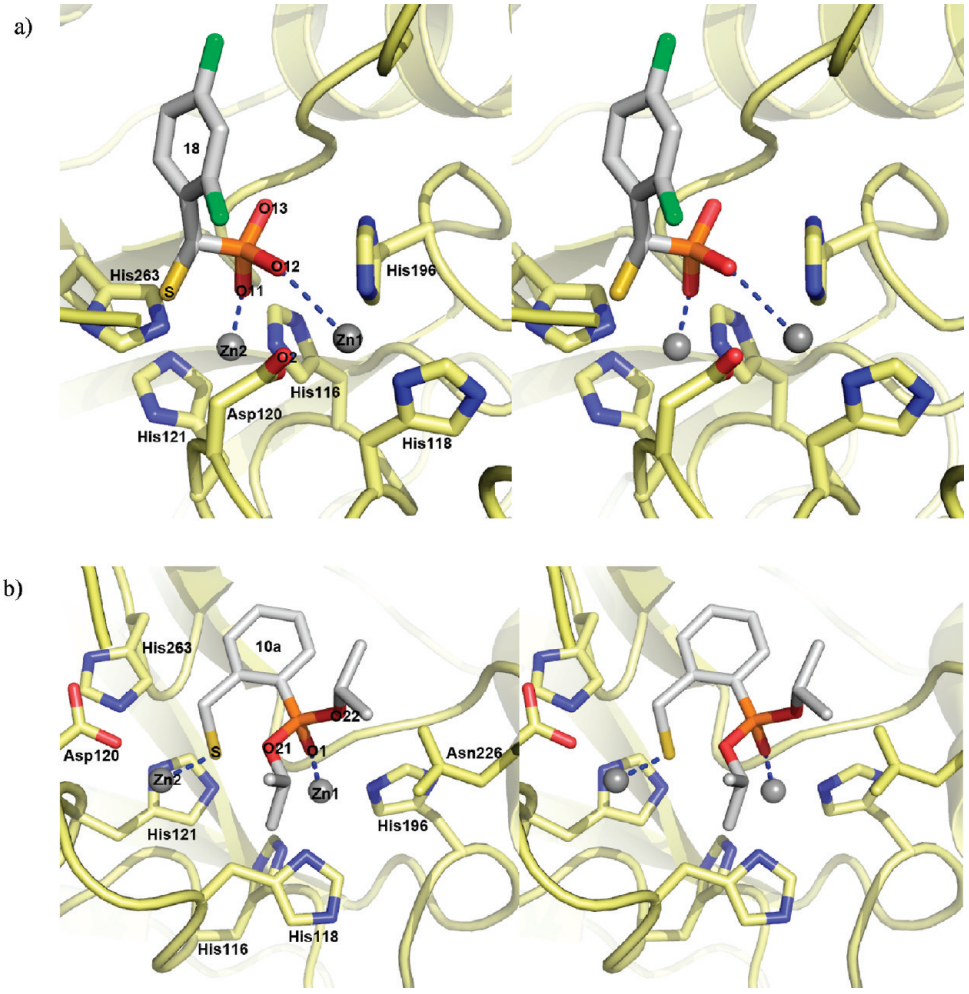

Figure 6. Molecular modeling of FEZ-1: stereoviews of all conformations. (a) Conformation representing the possible mode of binding of compound **18** to FEZ-1. The inhibitor interacts with Zn1 and Zn2 via two oxygen atoms (O11 and O12) of the phosphonato group. (b) Conformation representing the possible mode of binding of compound **10a** to FEZ-1. The inhibitor interacts with Zn1 via one oxygen atom (O1) of the phosphonato group and with Zn2 via the sulfanyl group.

point to two types of interactions with the enzyme depending of the complexed inhibitor. Indeed, in the case of **10a**, an interaction of the sulfur atom with the active site Zn^{2+} ion is observed, while **18** interacts with the Zn^{2+} ion via its phosphonato group. A similar situation is observed in the CphA−D-captopril complex (PDB code 2QDS) where the main interaction between D-captopril and the metal occurs via the inhibitor carboxylate group and not via the sulfanyl group of D-captopril.[11] However, a comparison of the CphA−**10a** and CphA−**18** complex structures with that previously reported for the carbapenem substrate[40] or for other inhibitors (PDB codes 2QDS and 2GKL)[11,50] reveals a general pattern composed of three important contacts: (i) contact to the Zn^{2+} ion, (ii) contact to the conserved Lys224 residue (directly or via a water molecule), and (iii) contact to Asn233 that stabilizes the Gly232-Asn233 loop closure. In this respect, it is not surprising that the simplest compound (**11a**) has a low K_i constant (2 μM) for CphA.

A short contact between the O1 of the phosphonato group and CE2 of the Phe156 residue (2.89 Å) is observed for **10a**. This kind of hydrogen bond can be observed when an aromatic or aliphatic carbon atom is polarized by an adjacent covalently bonded heteroatom, acidifying the CH hydrogen atoms.[51]

Previously, the crystal structures of the *Escherichia coli* alkaline phosphatase in interaction with a phosphoracetic acid (PAA) or a mercaptomethylphosphonate (MMP) inhibitor have also revealed the existence of different binding modes.[18] Those compounds differ only by the substitution of the carboxylate group of PAA by a sulfanyl group in MMP. The inhibitor PAA bridges the two Zn^{2+} ions of the enzyme via two of the three oxygen atoms of its phosphonato group, while the structure presenting the interaction between the alkaline phosphatase and MMP shows that the sulfanyl is a ligand of the first zinc ion with the phosphonato group directed out of the active site. The sulfanyl group then seems to be preferred as a ligand to the phosphonato group. However, the phosphonate is able to form three very strong salt bridges with both Zn^{2+} ions. MMP is a much more efficient inhibitor than PAA, suggesting that mercaptophosphonates would be more potent than phosphonates.

As we did not succeed in obtaining any MBL−inhibitor complex for subclasses B1 and B3, modeling studies were performed on the VIM-4 and FEZ-1 enzymes. Those studies revealed that the most probable binding mode of compound **18** occurs via its phosphonato group as obtained in the CphA−**18** crystallographic complex. For **10a**, the agreement is not so good. In the crystallographic data, the sulfanyl is interacting with the Zn^{2+} ion while the "best" model obtained for the CphA enzyme with molecular modeling favors an interaction between the phosphonato group and the Zn^{2+} ion. However, the structure observed by X-rays ranks among the three best ones obtained by modeling. Futhermore, the inhibitor−protein interaction in the

Table 5. Characterization of the Potential Binding Modes between FEZ-1 and **18** and **10a**[a]

parameter		**18** conformation 1		**10a** conformation 1	**10a** conformation 2
energy (kcal/mol)					
interacting energy		−115.45		−242.54	−161.96
distortion energy of compound **10a**		7.52		20.44	18.20
distance of interaction (Å)					
Zn1	His116	(5.14)		(4.24)	(4.56)
	His118	2.07		2.20	2.16
	His196	2.15		2.12	2.17
	18-S		**10a**-S		2.27
	18-O_{12}	2.82	**10a**-O_1	1.87	
Zn1−Zn2		4.52		3.18	6.49
Zn2	Asp120-O_1	1.94		1.93	1.93
	Asp120-O_2				2.01
	His121	(3.96)		(4.31)	(4.06)
	His263	2.17		(3.94)	(5.09)
	18-O_{11}	1.90	**10a**-S	2.29	
	Asp120-main chain			2.06	
	His118-main chain			2.05	
	His116	2.17			

[a] Distances in parentheses are too long for the residue to be a Zn^{2+} ligand. The interaction energy is the difference between the energy of the complex and the energies of its constituents in the complex geometry. The distortion energy is the sum of the distortion energies of the constituents, i.e., the difference between the energy of the constituents in the complex geometry and the energy of their optimized geometries.

crystallographic complex could be influenced by the crystal packing. For VIM-4 and FEZ-1, the most probable model of binding was characterized by two interactions between the enzyme and the inhibitor, S−Zn1 and O−Zn2 for VIM-4 and S−Zn2 and O−Zn1 for FEZ-1. The electrostatic surface potentials of VIM-4 and CphA indicate strongly cationic active site pockets which could select an interaction with the phosphonato group. In contrast FEZ-1 exhibits an anionic active site pocket that should have an impact on the interaction. The two methyl groups on phosphonate **10a** increase the size of this part of the molecule. The interaction of this inhibitor via its phosphonate seems to be impaired by its bulk, which could explain why the sulfanyl group is the main interacting group in this case and why the minimization process selects interactions occurring via both functions even if the protein is highly destabilized. On this basis, the sulfanyl interaction between **10a** and the MBLs seems to be the real interaction.

In conclusion, the investigation of mercaptophosphonate derivatives as MBL inhibitor has allowed us to find broad spectrum inhibitors active on representative members of all the three MBL subclasses. These compounds present K_i values in the same range as those of the compound previously described as a broad-spectrum MBL inhibitor by Liénard et al.[11] Moreover, on the basis of structural and modeling data, these phosphonate compounds could be improved further.

Experimental Section

Synthesis. General. Reaction progress was monitored by thin-layer chromatography (TLC) using Merck silica gel 60 aluminum sheets (F254). The plates were visualized either by UV light (254 nm) or by a solution of potassium permanganate. Column chromatography was performed using Merck silica gel Si 60 (40−63 μm). The quality of the solvents used was RS. THF was purified with a PURESOLV apparatus developed by Innovative Technology Inc. NMR spectra were recorded with a Bruker DPX 250 MHz or a Bruker DRX 400 MHz spectrometer. The peak patterns are indicated as follows: s, singlet; d, doublet; t, triplet; sept, septuplet; m, multiplet. Spectra were recorded with TMS as internal standard or with 85% phosphoric acid solution as external reference. The coupling constants (J) are reported in hertz (Hz). Mass spectra were obtained on a GC/MS Saturn 2000 spectrometer and HRMS data on a Waters QTOF microspectrometer. IR spectra were recorded with a Perkin-Elmer 16 PC FT-IR instrument. The purity of all tested inhibitors was assessed by elemental analysis or by HPLC analysis and found to be ≥95% (details are given in Supporting Information). A Waters PDA-HPLC instrument with a Waters XTerra MS-C18 (150 mm × 4.6 mm, 3.5 μm particle size) reversed-phase column was used for analytical HPLC analyses. The eluent was water/acetonitrile: 10/90, flow rate 1 mL/min. Elemental analysis was performed on a ThermoFinnigan NA 2500 apparatus. Melting points were measured with a Gallenkamp apparatus and are uncorrected.

Inhibitors **1a**, **1b**,[37] **11a**, and **12a**[35] have been synthesized and described previously. Synthesis and analytical data for inhibitors **13**, **10b**, **11b**, **12b**, **19**−**22** and additional spectroscopic data for compounds **8**, **9**, **10a**, **14**−**18** are given in Supporting Information.

Synthesis of Inhibitor 10a. Triethylammonium Diisopropyl Phosphorothioate (8). To a round-bottom flask equipped with a condenser diisopropyl phosphite (10.2 g, 1 equiv, 61.4 mmol) and sulfur (1.9 g, 1 equiv, 61.4 mmol) were added. Then triethylamine (15 mL) was added dropwise. The reaction is exothermic. After 30 min, when the mixture reached room temperature, the excess triethylamine was evaporated. The ammonium salt **8** was obtained as a brown viscous liquid and was used directly in the next step. Yield: quantitative. ^{31}P NMR (101.2 MHz, $CDCl_3$): δ 56.9. ^{1}H NMR (250 MHz, $CDCl_3$): δ 1.27 (d, 12H, $^3J_{HH}$ = 6.3 Hz); 1.35 (t, 9H, $^3J_{HH}$ = 7.3 Hz); 3.13 (q, 6H, $^3J_{HH}$ = 7.3 Hz); 4.60 (dsept, 2H, $^3J_{HH}$ = 6.1 Hz, $^3J_{HP}$ = 10.7 Hz); 12.25 (s, 1H). ^{13}C NMR (62.9 MHz, $CDCl_3$): δ 8.8; 23.9 (d, $^3J_{CP}$ = 4.7 Hz); 24.1 (d, $^3J_{CP}$ = 4.9 Hz); 45.6; 69.3 (d, $^2J_{CP}$ = 6.0 Hz).

Diisopropyl (2-Iodobenzyl)phosphorothioate (9). To a 250 mL round-bottom flask equipped with a condenser were added ammonium phosphorothioate **8** (9.9 g, 1 equiv, 33.1 mmol) and 2-iodobenzyl chloride (10.0 g, 1.2 equiv, 39.7 mmol) in toluene (100 mL). The mixture was heated for 14 h, then allowed to reach room temperature. The organic layer was washed with a 5% solution of sodium thiosulfate, separated, dried over $MgSO_4$, filtered, and evaporated. The brown oil was purified by flash chromatography (eluent: pentane/AcOEt 60/40) to afford compound **9** as a colorless liquid. Yield: 94%. ^{31}P NMR (101 MHz, $CDCl_3$): δ 24.8. ^{1}H NMR (250 MHz, $CDCl_3$): δ 1.26 (d, 6H, $^3J_{HH}$ = 6.2 Hz); 1.29 (d, 6H, $^3J_{HH}$ = 6.2 Hz); 4.16 (d, 2H, $^3J_{HP}$ = 13.8 Hz); 4.69 (dsept, 2H, $^3J_{HH}$ = 6.2 Hz, $^3J_{HP}$ = 9.1 Hz); 6.94 (dt, 1H, $^3J_{HH}$ = 7.7 Hz, $^4J_{HH}$ = 1.7 Hz); 7.29 (dt, 1H, $^3J_{HH}$ = 7.5 Hz, $^4J_{HH}$ = 1.7 Hz); 7.51 (dd, 1H, $^3J_{HH}$ = 7.6 Hz, $^3J_{HH}$ = 1.6 Hz); 7.82 (dd, 1H, $^3J_{HH}$ = 7.9 Hz, $^4J_{HH}$ = 1.1 Hz). ^{13}C NMR (62.9 MHz, $CDCl_3$): δ 23.9 (d, $^3J_{CP}$ = 5.7 Hz); 24.1 (d, $^3J_{CP}$ = 3.8 Hz); 40.9 (d, $^2J_{CP}$ = 3.8 Hz); 73.1 (d, $^2J_{CP}$ = 6.3 Hz); 100.6; 128.9; 129.7; 131.1; 140.0; 140.7 (d, $^3J_{CP}$ = 5.0 Hz).

Diisopropyl 2-(Sulfanylmethyl)phenylphosphonate (10a). In a round-bottom flask, under nitrogen, a solution of 2-iodobenzyl phosphorothioate **9** (508 mg, 1 equiv, 1.2 mmol) in 5 mL of THF was added dropwise to a solution of t-BuLi (1.4 mL, 2 equiv, 1.7 M in hexane, 2.4 mmol) in THF (20 mL) at −78 °C. After the mixture was stirred for 2 h at −78 °C, the reaction was quenched at −10 °C with 10 mL of HCl (2 N). The aqueous layer was extracted with Et_2O (2 × 15 mL). Then the organic layers were separated, dried on $MgSO_4$, filtered, and evaporated. The obtained product was purified by chromatography on silica gel (eluent: pentane/AcOEt 50/50) to give compound **10** as a yellow oil (210 mg, 61%). ^{31}P NMR

(101.2 MHz, $CDCl_3$): δ 17.6. ^{1}H NMR (250 MHz, $CDCl_3$): δ 1.26 (d, 3H, $^3J_{HH}$ = 6.2 Hz, CH_3); 1.27 (d, 3H, $^3J_{HH}$ = 6.2 Hz); 1.38 (d, 3H, $^3J_{HH}$ = 6.2 Hz); 1.39 (d, 3H, $^3J_{HH}$ = 6.2 Hz); 2.21 (t, 1H, $^3J_{HH}$ = 8.4 Hz); 4.05 (d, 2H, $^3J_{HH}$ = 8.4 Hz); 4.75 (dsept, 2H, $^3J_{HH}$ = 6.2 Hz, $^3J_{HP}$ = 9.6 Hz); 7.27−7.32 (m, 1H); 7.45−7.49 (m, 2H); 7.89 (ddd, 1H, $^3J_{HP}$ = 14.3 Hz, $^3J_{HH}$ = 6.9 Hz, $^4J_{HH}$ = 0.7 Hz). ^{13}C NMR (62.9 MHz, $CDCl_3$): δ 24.2 (d, $^3J_{CP}$ = 5.0 Hz); 24.4 (d, $^3J_{CP}$ = 3.8 Hz); 27.3 (d, $^3J_{CP}$ = 3.1 Hz); 71.3 (d, $^2J_{CP}$ = 6.3 Hz); 126.8 (d, $^3J_{CP}$ = 14.4 Hz); 127.6 (d, $^1J_{CP}$ = 185.6 Hz); 130.8 (d, $^3J_{CP}$ = 14.5 Hz); 133.0 (d, $^4J_{CP}$ = 2.5 Hz); 133.8 (d, $^2J_{CP}$ = 9.4 Hz); 145.5 (d, $^2J_{CP}$ = 9.4 Hz).

Synthesis of Inhibitor 18. Diisopropyl α-Hydroxy(2,4-dichlorobenzyl)phosphonate (14). A mixture of diisopropyl phosphite (1.66 g, 10 mmol, 1 equiv), 2,4-dichlorobenzaldehyde (1.75 g 10 mmol, 1 equiv), and triethylamine (7 mL, 50 mmol, 5 equiv) was heated at reflux for 3 h. After addition of HCl 4 N (10 mL), the resulting mixture was extracted with CH_2Cl_2 (2 × 20 mL). The organic layers were dried on $MgSO_4$ and concentrated under reduced pressure to afford hydroxyphosphonate **14** as a white powder, which was used directly in the next step. Yield: 90%. Mp = 92 °C. ^{31}P NMR ($CDCl_3$, 101.25 MHz): δ 18.9. ^{1}H NMR (400 MHz, $CDCl_3$): δ 1.10 (d, $^3J_{HH}$ = 6.1 Hz, 3H); 1.18 (d, $^3J_{HH}$ = 6.1 Hz, 3H); 1.20 (d, $^3J_{HH}$ = 6.1 Hz, 3H); 1.21 (d, $^3J_{HH}$ = 6.1 Hz, 3H); 4.55 (m, 1H); 4.65 (m, 1H, CHOP); 5.33 (d, $^2J_{HP}$ = 12.0 Hz, 1H); 7.22 (dd, $^3J_{HH}$ = 8.4 Hz, J = 2.0 Hz, 1H); 7.31 (dd, J = 1.2 Hz, J = 2.0 Hz, 1H); 7.59 (dd, $^3J_{HH}$ = 8.4 Hz, J = 2.4 Hz, 1H). ^{13}C NMR (100.62 MHz, $CDCl_3$): δ 23.4 (d, $^3J_{CP}$ = 3.2 Hz); 23.8 (d, $^3J_{CP}$ = 3.8 Hz); 23.9 (d, $^3J_{CP}$ = 3.8 Hz); 24.2 (d, $^3J_{CP}$ = 3.8 Hz); 66.8 (d, $^1J_{CP}$ = 162.8 Hz); 72.0 (d, $^2J_{CP}$ = 7.7 Hz); 72.5 (d, $^2J_{CP}$ = 7.5 Hz); 127.1 (d, J_{CP} = 3.1 Hz); 128.8 (d, J_{CP} = 2.2 Hz); 130.3 (d, J_{CP} = 4.1 Hz); 133.7 (d, J_{CP} = 8.1 Hz); 134.14 (d, J_{CP} = 3.9 Hz); 134.16.

Diisopropyl α-(*p*-Nitrobenzenesulfonyloxy)(2,4-dichlorobenzyl)phosphonate (15). *p*-Nitrobenzenesulfonyl chloride (1.13 g, 5.1 mmol, 1.2 equiv), NEt_3 (1.5 mL), and 4-(*N*,*N*-dimethylamino)pyridine (DMAP) (10 mg/mmol **14**, 43 mg) were added to a solution of hydroxyphosphonate **14** (1.46 g, 4.3 mmol, 1 equiv) in dry CH_2Cl_2 (20 mL) under nitrogen at 0 °C. The reaction mixture was stirred at room temperature for 7 h. After the addition of a mixture of water (10 mL) and 12 N HCl (15 mL), the organic phase was separated and the aqueous phase was extracted twice with CH_2Cl_2 (10 mL). The combined organic phases were washed with a saturated aqueous solution of $NaHCO_3$, dried over $MgSO_4$, and concentrated under reduced pressure. The crude product **15** was obtained as a white solid and was used directly in the next step. Yield: 95%. Mp = 109 °C. ^{31}P NMR ($CDCl_3$, 161.97 MHz): δ 11.1. ^{1}H NMR (400 MHz, $CDCl_3$): δ 0.98 (d, $^3J_{HH}$ = 6.4 Hz, 3H); 1.18 (d, $^3J_{HH}$ = 6.4 Hz, 3H); 1.21 (d, $^3J_{HH}$ = 6.4 Hz, 3H); 1.24 (d, $^3J_{HH}$ = 6.4 Hz, 3H); 4.49 (m, 1H); 4.74 (m, 1H); 6.07 (d, $^2J_{HP}$ = 16.0 Hz, 1H); 7.02 (dd, $^3J_{HH}$ = 8.8 Hz, J = 2.0 Hz, 1H); 7.22 (dd, J = 1.2 Hz, J = 2.0 Hz, 1H); 7.37 (dd, $^3J_{HH}$ = 8.4 Hz, J = 2.4 Hz, 1H); 7.94 (AA BB system, J = 8.9, 4H). ^{13}C NMR (100.62 MHz, $CDCl_3$): δ 23.3 (d, $^3J_{CP}$ = 3.2 Hz); 23.7 (d, $^3J_{CP}$ = 3.8 Hz); 24.0 (d, $^3J_{CP}$ = 3.8 Hz); 24.1 (d, $^3J_{CP}$ = 3.8 Hz); 73.2 (d, $^2J_{CP}$ = 7.1 Hz); 73.6 (d, $^2J_{CP}$ = 7.1 Hz); 73.8 (d, $^1J_{CP}$ = 175.6 Hz); 124.0; 127.5; 128.3; 128.5; 129.3; 131.3 (d, J_{CP} = 3.5 Hz); 134.3 (d, J_{CP} = 8.4 Hz); 136.2 (d, J_{CP} = 3.1 Hz); 141.9; 150.6.

Diisopropyl α-Thiocyanato(2,4-dichlorobenzyl)phosphonate (16). A mixture of phosphonate **15** (1.58 g, 3.0 mmol, 1 equiv), KSCN (1.16 g, 12 mmol, 4 equiv), and 18-crown-6 (50 mg/mmol of **15**, 150 mg) in dry acetonitrile (30 mL) was refluxed for 40 h under nitrogen. Then acetonitrile was evaporated, and after addition of water (20 mL), the mixture was extracted with AcOEt (3 × 20 mL). The combined organic layers were dried with $MgSO_4$ and concentrated under reduced pressure. The crude product **16** was obtained as a yellow oil and was used directly in the next step. Yield: 79%. ^{31}P NMR ($CDCl_3$, 161.97 MHz): δ 14.5. ^{1}H NMR (400 MHz, $CDCl_3$): δ 0.99 (d, $^3J_{HH}$ = 6.0 Hz, 3H); 1.18 (d, $^3J_{HH}$ = 6.1 Hz, 3H); 1.24 (d, $^3J_{HH}$ = 6.1 Hz, 6H); 4.53 (m, 1H); 4.78 (m, 1H); 5.00 (d, $^2J_{HP}$ = 19.6 Hz, 1H); 7.28 (dd, $^3J_{HH}$ = 8.8 Hz, J = 2.0 Hz, 1H); 7.40 (dd, J = 1.2 Hz, J = 2.0 Hz, 1H); 7.75 (dd, $^3J_{HH}$ = 8.8 Hz, J = 2.0 Hz, 1H). ^{13}C NMR (100.62 MHz, $CDCl_3$): δ 23.2 (d, $^3J_{CP}$ = 3.6 Hz); 23.8 (d, $^3J_{CP}$ = 3.6 Hz); 24.0 (d, $^3J_{CP}$ = 3.6 Hz,); 24.1 (d, $^3J_{CP}$ = 3.6 Hz); 42.7 (d, $^1J_{CP}$ = 150.6 Hz); 73.5 (d, $^2J_{CP}$ = 7.1 Hz); 73.8 (d, $^2J_{CP}$ = 7.3 Hz); 109.9 (d, $^2J_{CP}$ = 9.5 Hz), 128.1 (d, J_{CP} = 2.0 Hz); 129.6 (d, J_{CP} = 1.2 Hz); 129.7; 131.5 (d, J_{CP} = 3.7 Hz); 135.0 (d, J_{CP} = 9.8 Hz); 135.1 (d, J_{CP} = 2.0 Hz).

Diisopropyl α-Sulfanyl(2,4-dichlorobenzyl)phosphonate (17). A solution of thiocyanatophosphonate **16** (382 mg, 1 mmol, 1 equiv) in EtOH 95% (10 mL) was added dropwise to a stirred solution of $NaBH_4$ (190 mg, 5 mmol, 5 equiv) in EtOH 95% (10 mL) at room temperature. The mixture was stirred for 2 h (the reaction was monitored by TLC), then poured into a cooled solution of 2 N HCl (10 mL) at 0 °C and extracted with AcOEt (3 × 20 mL). The combined organic phases were dried ($MgSO_4$) and concentrated under reduced pressure. The crude product was purified by flash chromatography (pentane/AcOEt 1/1, R_f = 0.5) to give **17** as a pale-yellow oil, which was stored under argon in the freezer to avoid oxidation to disulfide. Yield: 64%. ^{31}P NMR ($CDCl_3$, 161.97 MHz): δ 20.2. ^{1}H NMR (400 MHz, $CDCl_3$): δ 0.94 (d, $^3J_{HH}$ = 6.4 Hz, 3H); 1.18 (d, $^3J_{HH}$ = 6.4 Hz, 3H); 1.24 (d, $^3J_{HH}$ = 6.4 Hz, 3H); 1.31 (d, $^3J_{HH}$ = 6.4 Hz, 3H); 2.53 (dd, $^3J_{HH}$ = 9.2, $^3J_{HP}$ = 11.6, 1H); 4.47 (m, 2H); 4.76 (m, 1H); 7.20 (dd, J = 2.0 Hz, $^3J_{HH}$ = 8.4 Hz, 1H); 7.31 (dd, J = 1.2 Hz, J = 2.0 Hz, 1H); 7.67 (dd, $^3J_{HH}$ = 8.4 Hz, J = 2.0 Hz, 1H). ^{13}C NMR (100.62 MHz, $CDCl_3$): δ 23.2 (d, $^3J_{CP}$ = 3.1 Hz); 23.7 (d, $^3J_{CP}$ = 3.7 Hz); 24.1 (d, $^3J_{CP}$ = 3.1 Hz); 24.2 (d, $^3J_{CP}$ = 3.7 Hz); 33.8 (d, $^1J_{CP}$ = 151.0 Hz); 72.4 (d, $^2J_{CP}$ = 7.3 Hz); 72.6 (d, $^2J_{CP}$ = 7.4 Hz); 127.6 (d, J_{CP} = 2.3 Hz); 129.0 (d, J_{CP} = 1.2 Hz); 131.1 (d, J_{CP} = 3.9 Hz); 133.7 (d, J_{CP} = 3.1 Hz); 134.1 (d, J_{CP} = 9.9 Hz); 134.4 (d, J_{CP} = 1.4 Hz).

α-Sulfanyl(2,4-dichlorobenzyl)phosphonic Acid (18). To a stirred solution of 1-sulfanylphosphonate **17** (165 mg, 1 equiv, 0.46 mmol) in CH_2Cl_2 (2 mL) was added dropwise Me_3SiBr (0.5 mL, 3.3 mmol, 7 equiv). The mixture was stirred for 2 days at room temperature. The volatile products were evaporated. The residue was dissolved in a mixture of CH_2Cl_2/MeOH (3/1) and stirred for 3 h. Then the solvents evaporated to give the mercaptophosphonic acid **18** as a hygroscopic white paste (89 mg, 72%). ^{31}P NMR (161.97 MHz, D_2O/MeOD 80/20): δ 20.0. ^{1}H NMR (400.13 MHz, D_2O/MeOD 80/20): δ 4.54 (d, $^2J_{HP}$ = 19.6, 1H); 7.23 (dd, $^3J_{HH}$ = 8.8 Hz, J = 1.6 Hz, 1H); 7.38 (s, 1H, H); 7.67 (dd, $^3J_{HH}$ = 8.8 Hz, J = 1.6 Hz, 1H). ^{13}C NMR (100.62 MHz, D_2O/MeOD 80/20): δ 34.4 (d, $^1J_{CP}$ = 140.8 Hz); 127.6 (d, J_{CP} = 2.2 Hz); 128.8 (d, J_{CP} = 1.3 Hz); 130.7 (d, J_{CP} = 3.8 Hz); 133.2 (d, J_{CP} = 2.9 Hz); 133.6 (d, J_{CP} = 8.6 Hz); 135.2 (d, J_{CP} = 2.5 Hz).

Chemicals. Buffers and bovine serum albumin (BSA) were obtained from Sigma-Aldrich (Steinheim, Germany). Dimethyl sulfoxide (DMSO) and $ZnCl_2$ were purchased from Merck (Darmstadt, Germany). Imipenem ($\Delta\varepsilon_{300} = -9000$ M^{-1} cm^{-1}) was from Merck Sharpe and Dohme Research Laboratories (Rahway, NJ). Nitrocefin ($\Delta\varepsilon_{482} = -15\,000$ M^{-1} cm^{-1}) was from Oxoid LTD (Basingstoke, U.K.).

Enzyme Production and Purification. The CphA, CphA N220G, CphA N116H-N220G,[41] VIM-4,[43] L1,[52] and FEZ-1[32] MBLs were produced and purified as described previously.

Determination of the Inhibition Constant. Solutions of **18** and **1b** (100 mM) were prepared in DMSO before dilution with a convenient buffer containing 20 μg/mL BSA and 50 μM $ZnCl_2$ when indicated. The buffers were 10 mM HEPES, pH 7.2, for VIM-4, 15 mM cacodylate, pH 6.5, for CphA, and 20 mM HEPES, pH 7.0, for L1. The inhibitors **1a**, **10a**, **10b**, **11a**, **11b**, **12a**, **12b**, **13**, **19**, **20**, **21**, and **22** were prepared as 100 mM stock solutions directly into the proper buffer. The VIM-4 subclass B1 enzyme and the L1 subclass B3 enzyme were tested without and with additional Zn^{2+} (50 μM final concentration) in the buffer in order to detect a potential chelating effect of the inhibitor. The study of the subclass B2 enzyme CphA was done without addition of Zn^{2+} to the buffer, since this subclass only requires one Zn^{2+} for its activity and is inhibited by the addition of Zn^{2+}. VIM-4, CphA, and L1 enzymes were used at fixed concentrations between

0.2 and 0.8 nM. The enzyme and inhibitor (100 μM) were preincubated for 30 min at 37 °C before the substrate was added. Hydrolysis of imipenem (CphA and L1) or nitrocefin (VIM-4) was monitored by following the variation in absorbance at 300 or 482 nm, respectively, using a Uvikon 860 spectrophotometer. The activity was tested using an initial rate of three samples without inhibitor. The initial rate conditions were used to study the inhibition by using the Hanes linearization of the Henri−Michaelis equation. The competitive inhibition constant, K_i, was calculated using the following equation:[53]

$$v = \frac{V_{max} S}{S + K_m(1 + I/K_i)}$$

For compounds **1b** and **18**, it was checked that the rate in absence of inhibitor remained the same upon addition of 1% DMSO.

Crystallography. Crystallization of the CphA−10a and CphA−18 Complexes and Data Collection. Crystallization of the N220G CphA was performed as described previously.[39] Before data collection, 1 μL of 1.5 mM **10a** or **18** was added to the drops containing the crystals and soaked. After several days, the crystals were soaked with 1 μL of inhibitor solution again. For data collection, crystals were transferred to a cryoprotectant solution containing reservoir solution supplemented with 30% (v/v) glycerol. The mounted crystals were flash-frozen in a liquid nitrogen stream. Nearly complete X-ray data sets were collected using an in-house Bruker FR591 rotating anode X-ray generator and a Mar345dtb detector. Diffraction data were processed with XDS[54] and scaled with SCALA from the CCP4 suite[55] (Table 1).

Structure Determination and Refinement. Initial phases for the CphA−**10a** and CphA−**18** complex structures were generated by molecular replacement, using the structure of the wild-type CphA as a starting model (Protein Data Bank accession code 1X8G). Molecular replacement was performed with Phaser.[56] The obtained molecular replacement models were rebuilt with ARP/wARP automatically.[57] On inspection, the first electron density map clearly showed the presence of additional density in the active site, the form of which looked like an inhibitor molecule. After most of the protein main chain and side chain atoms and most of the water molecules were built and refined, compounds **10a** and **18** were modeled into the map. Conformational torsion angle restraints and charge assignments for the **10a** and **18** molecules were obtained using CCP4i Libcheck.

The structures were refined in a cyclic process including manual inspection of the electron density with Coot[58] and refinement with Refmac.[59] The refinement to convergence was done with isotropic *B*-values and using translation/libration/screw (TLS) parameter. The positions of the Zn^{2+} ions and the positions of the sulfur and phosphorus atoms were verified by calculating anomalous maps. Alternative conformations were modeled for a number of side chains, and occupancies were adjusted to yield similar *B*-values for the disordered conformations. Refinement statistics are shown in Table 1.

Protein Structure Accession Number. Coordinates and structure factors for CphA−**10a** and CphA−**18** complexes have been deposited in the Protein Data Bank with the respective accession codes 3IOF and 3IOG.

Molecular Modeling. Our methodology was chosen to try to highlight differences between distinct binding modes involving Zn^{2+}−sulfanyl or Zn^{2+}−phosphonate interactions. The VIM-4−**10a** and VIM-4−**18** complex models were based on the three-dimensional structure of VIM-4 enzyme[43] (2WHG). This 3D structure has the advantage of possessing a citrate anion in the active site of the protein. The active site is then in an ideal "open conformation" to fit a compound. The starting position of the complexes between the enzyme and the inhibitor was built by empirically docking the substrate in the cavity with the program InsightII.[60] Given the chemical nature of the inhibitor, interactions between the Zn^{2+} ions and two chemical groups (the phosphonato and the sulfanyl groups) were possible. However, it has been demonstrated for previous MBL inhibitor possessing a sulfanyl (thiol) group that the inhibition mainly occurs via an interaction between Zn^{2+} ions and the sulfanyl function.[61] For the modeling studies, we have thus privileged this interaction. In consequence, two orientations of the inhibitor in the active site cavity were chosen as starting positions: the sulfanyl in interaction with the Zn^{2+} ion in the "histidine" site (Zn1) and the sulfanyl in interaction with the Zn^{2+} ion in the "cysteine" site (Zn2). We have used charged phosphonato and sulfanyl groups because preliminary studies had confirmed that a deprotonated function was necessary to avoid repulsion by the Zn^{2+} ion. Two other models of VIM-4 in complex with **10a** and **18** were built using the positions of each compound in the CphA−**10a** and CphA−**18** crystallographic complexes. The different complexes were soaked in a 5 Å layer of water molecules. The geometry was first fully optimized at the molecular mechanics (MM) level[62] with a maximum force convergence threshold of 0.02 kcal mol^{-1} Å^{-1} and then submitted to a dynamics simulation at 300 K during 100 ps. The chosen force field was Amber,[63,64] the relative dielectric constant was set to 1, and the programs used were InsightII and Discover running on a Pentium 4 3.4 GHz under Unix Debian. The Zn^{2+} ions and the inhibitors are not recognized as such by the Amber force field. Thus, each atom must be defined manually as an atom-type recognized by Amber, such as for instance CA for aromatic carbons or CU for the Zn^{2+} atoms which were dealt with as ions whose net charge had to be defined. The net charges of the inhibitor and the Zn^{2+} ions were determined at the quantum chemistry level, at the RHF/6-31+G** level with the Gaussian 03 program.[65] No heating or equilibration step was used in the dynamics simulation, but the 3D structure submitted to the final geometry optimization was chosen as the average conformation built on the end (50 ps) of the simulation dynamics.

In order to validate the achieved VIM-4−**18** or VIM-4−**10a** conformations, the CphA−**10a** and CphA−**18** complexes were optimized and a study was performed using the initial orientations for the inhibitor previously used for VIM-4. Energy minimization and dynamic simulation were conducted as described above.

Finally, FEZ-1−**10a** and FEZ-1−**18** complex models were built using the structure of FEZ-1 in interaction with D-captotril (1JT1), which also presented a wide active site ideal for inhibitor docking. The molecular models of FEZ-1 were based on the docking on VIM-4 and on the structural conformation of the inhibitors in CphA. Energy minimization and dynamic simulation were performed as described above.

Acknowledgment. C.B. is a postdoctoral researcher of the FRS/FNRS (Belgium). P.L. is a fellow of the "Fonds pour la Formation à la Recherche dans l'Industrie et l'Agriculture" (FRIA; Brussels, Belgium). We thank Prof. Paulette Charlier, Dr. Frédéric Kerff, and Raphaël Hermann (CIP, University of Liège, Belgium) for their help with the FEZ-1 crystals. The work in Liège was supported by the Interuniversity Attraction Poles (IAP P6/19), Belgian Federal Government, and Grants 2.4511.06, 2.4561.07, 2.4548.10 from the FRS/FNRS (Brussels, Belgium) and Lot. Nat. 9.4538.03. The work in Aachen was supported by the European Regional Development Fund (ERDF) and the European Union ("Die Europäische Kommission investiert in Ihre Zukunft").

Supporting Information Available: Purities of inhibitors **1a**, **1b**, **10a**, **10b**, **11a**, **11b**, **12a**, **12b**, **13**, **18**−**22** from HPLC or elemental analysis; additional spectroscopic data for compounds **8**, **9**, **10a**, **14**−**18**; synthesis and analytical details for inhibitors **10b**, **11b**, **12b**, **13**, **19**−**22**. This material is available free of charge via the Internet at http://pubs.acs.org.

References

(1) Ambler, R. P. The structures of beta-lactamases. *Philos Trans. R. Soc. London, Ser. B* **1980**, *289*, 321–331.
(2) Galleni, M.; Lamotte-Brasseur, J.; Rossolini, G. M.; Spencer, J.; Dideberg, O.; Frère, J. M.; The Metallo-β-lactamase Working Group. Standard numbering scheme for class B β-lactamases. *Antimicrob. Agents Chemother*. **2001**, *45*, 660–663.
(3) Garau, G.; Garcia-Saez, I.; Bebrone, C.; Anne, C.; Mercuri, P. S.; Galleni, M.; Frère, J. M.; Dideberg, O. Update of the standard numbering scheme for class B β-lactamases. *Antimicrob. Agents Chemother*. **2004**, *48*, 2347–2349.
(4) Frère, J. M.; Galleni, M.; Bush, K.; Dideberg, O. Is it necessary to change the classification of beta-lactamases? *J. Antimicrob. Chemother*. **2005**, *55*, 1051–1052.
(5) Bebrone, C. Metallo-beta-lactamases (classification, activity, genetic organization, structure, zinc coordination) and their superfamily. *Biochem. Pharmacol*. **2007**, *74*, 1686–1701.
(6) Prosperi-Meys, C.; Llabres, G.; de Seny, D.; Soto, R. P.; Valladares, M. H.; Laraki, N.; Frère, J. M.; Galleni, M. Interaction between class B beta-lactamases and suicide substrates of active-site serine beta-lactamases. *FEBS Lett*. **1999**, *443*, 109–111.
(7) Toney, J. H.; Moloughney., J. G. Metallo-beta-lactamase inhibitors: promise for the future? *Curr. Opin. Invest. Drugs* **2004**, *5*, 823–826.
(8) Mollard, C.; Moali, C.; Papamicael, C.; Damblon, C.; Vessilier, S.; Amicosante, G.; Schofield, C. J.; Galleni, M.; Frère, J. M.; Roberts, G. C. Thiomandelic acid, a broad spectrum inhibitor of zinc beta-lactamases: kinetic and spectroscopic studies. *J. Biol. Chem*. **2001**, *276*, 45015–45023.
(9) Payne, D. J.; Bateson, J. H.; Gasson, B. C.; Proctor, D.; Khushi, T.; Farmer, T. H.; Tolson, D. A.; Bell, D.; Skett, P. W.; Marshall, A. C.; Reid, R.; Ghosez, L.; Combret, Y.; Marchand-Brynaert, J. Inhibition of metallo-beta-lactamases by a series of mercaptoacetic acid thiol ester derivatives. *Antimicrob. Agents Chemother*. **1997**, *41*, 135–140.
(10) Heinz, U.; Bauer, R.; Wommer, S.; Meyer-Klaucke, W.; Papamichaels, C.; Bateson, J.; Adolph, H. W. Coordination geometries of metal ions in d- or l-captopril-inhibited metallo-beta-lactamases. *J. Biol. Chem*. **2003**, *278*, 20659–20666.
(11) Liénard, B. M. R.; Garau, G.; Horsfall, L.; Karsisiotis, A. I.; Damblon, C.; Lassaux, P.; Papamicael, G.; Roberts, C. K.; Galleni, M.; Dideberg, O.; Frère, J. M.; Schofield, C. J. Structural basis for the broad-spectrum inhibition of metallo-β-lactamases by thiols. *Org. Biomol. Chem*. **2008**, *6*, 2282–2294.
(12) Schwarzenbach, G.; Ackermann, H.; Ruchstuhl, P. *Helv. Chim. Acta* **1949**, *32*, 1175.
(13) (a) Gulea, M.; Masson, S. Recent Advances in the Chemistry of Difunctionalized Organo-Phosphorus and -Sulfur Compounds. In *New Aspects in Phosphorus Chemistry III*; Majoral, M., et al., Eds.; Topics in Current Chemistry, Vol. 229; Springer: Berlin, 2003; pp 161−198 (b) Gulea, M.; Gaumont, A.-C. Synthesis of Phosphorus-Substituted Sulfur Heterocycles. In *Targets in Heterocyclic Systems*; Attanasi, O. A., Spinelli, D., Eds.; Springer and Società Chimica Italiana: New York and Rome, 2008; Vol. 12, pp 328−348.
(14) Rahil, J.; Pratt, R. F. Phosphonate monoesters inhibitors of class A beta-lactamases. *Biochem. J*. **1991**, *275*, 793–795.
(15) Li, N.; Rahil, J.; Wright, M. E.; Pratt, R. F. Structure−activity of the inhibition of serine beta-lactamases by phosphonate monoesters. *Bioorg. Med. Chem*. **1997**, *5*, 1583–1588.
(16) Adediran, S. A.; Nukaga, M.; Baurin, S.; Frère, J. M.; Pratt, R. F. Inhibition of class D beta-lactamases by acyl-phosphates and phosphonates. *Antimicrob. Agents Chemother*. **2005**, *49*, 4410–4419.
(17) Myers, J. K.; Antonelli, S. M.; Widlanski, T. S. Motifs for metallophosphatase inhibition. *J. Am. Chem. Soc*. **1997**, *119*, 3163–3164.
(18) Holtz, K. M.; Stec, B.; Myers, J. K.; Antonelli, S. M.; Widlanski, T. S.; Kantrowitz, E. R. Alternate modes of binding in two crystal structures of alkaline phosphatase−inhibitor complexes. *Protein Sci*. **2000**, *9*, 907–915.
(19) Pournaras, S.; Tsakris, A.; Maniati, M.; Tzouvelekis, L. S.; Maniatis, A. N. Novel variant (bla(VIM-4)) of the metallo-beta-lactamase gene bla(VIM-1) in a clinical strain of *Pseudomonas aeruginosa*. *Antimicrob. Agents Chemother*. **2002**, *46*, 4026–4028.
(20) Massidda, O.; Rossolini, G. M.; Satta, G. The *Aeromonas hydrophila* cphA gene: molecular heterogeneity among class B metallo-beta-lactamases. *J. Bacteriol*. **1991**, *173*, 4611–4617.
(21) Walsh, T. R.; Hall, L.; Assinder, S. J.; Nichols, W. W.; Cartwright, S. J.; MacGowan, A. P.; Bennett, P. M. Sequence analysis of the L1 metallo-beta-lactamase from *Xanthomonas maltophilia*. *Biochim. Biophys. Acta* **1994**, *1218*, 199–201.
(22) Toleman, M. A.; Simm, A. M.; Murphy, T. A.; Gales, A. C.; Biedenbach, D. J.; Jones, R. N.; Walsh, T. R. Molecular characterization of SPM-1, a novel metallo-beta-lactamase isolated in Latin America: report from the SENTRY antimicrobial surveillance programme. *J. Antimicrob. Chemother*. **2002**, *50*, 673–679.
(23) Lee, K.; Yum, J. H.; Yong, D.; Lee, H. M.; Kim, H. D.; Docquier, J. D.; Rossolini, G. M.; Chong, Y. Novel acquired metallo-beta-lactamase gene, bla(SIM-1), in a class 1 integron from *Acinetobacter baumannii* clinical isolates from Korea. *Antimicrob. Agents Chemother*. **2005**, *49*, 4485–4491.
(24) Castanheira, M.; Toleman, M. A.; Jones, R. N.; Schmidt, F. J.; Walsh, T. R. Molecular characterization of a beta-lactamase gene, blaGIM-1, encoding a new subclass of metallo-beta-lactamase. *Antimicrob. Agents Chemother*. **2004**, *48*, 4654–4661.
(25) Osano, E.; Arakawa, Y.; Wacharotayankun, R.; Ohta, M.; Horii, T.; Ito, H.; Yoshimura, F.; Kato, N. Molecular characterization of an enterobacterial metallo-beta-lactamase found in a clinical isolate of *Serratia marcescens* that shows imipenem resistance. *Antimicrob. Agents Chemother*. **1994**, *38*, 71–78.
(26) Pournaras, S.; Maniati, M.; Petinaki, E.; Tzouvelekis, L. S.; Tsakris, A.; Legakis, N. J.; Maniatis, A. N. Hospital outbreak of multiple clones of *Pseudomonas aeruginosa* carrying the unrelated metallo-beta-lactamase gene variants blaVIM-2 and blaVIM-4. *J. Antimicrob. Chemother*. **2003**, *51*, 1409–1414.
(27) Libisch, B.; Gacs, M.; Csiszár, K.; Muzslay, M.; Rókusz, L.; Füzi, M. Isolation of an integron-borne blaVIM-4 type metallo-beta-lactamase gene from a carbapenem-resistant *Pseudomonas aeruginosa* clinical isolate in Hungary. *Antimicrob. Agents Chemother*. **2004**, *48*, 3576–3578.
(28) Luzzaro, F.; Docquier, J. D.; Colinon, C.; Endimiani, A.; Lombardi, G.; Amicosante, G.; Rossolini, G. M.; Toniolo, A. Emergence in *Klebsiella pneumoniae* and *Enterobacter cloacae* clinical isolates of the VIM-4 metallo-beta-lactamase encoded by a conjugative plasmid. *Antimicrob. Agents Chemother*. **2004**, *48*, 648–650.
(29) Giske, C. G.; Rylander, M.; Kronvall, G. VIM-4 in a carbapenem-resistant strain of *Pseudomonas aeruginosa* isolated in Sweden. *Antimicrob. Agents Chemother*. **2004**, *47*, 3034–3035.
(30) Patzer, J.; Toleman, M. A.; Deshpande, L. M.; Kamińska, W.; Dzierzanowska, D.; Bennett, P. M.; Jones, R. N.; Walsh, T. R. *Pseudomonas aeruginosa* strains harbouring an unusual blaVIM-4 gene cassette isolated from hospitalized children in Poland (1998−2001). *J. Antimicrob. Chemother*. **2004**, *53*, 451–456.
(31) Ktari, S.; Arlet, G.; Mnif, B.; Gautier, V.; Mahjoubi, F.; Ben Jmeaa, M.; Bouaziz, M.; Hammami, A. Emergence of multidrug-resistant *Klebsiella pneumoniae* isolates producing VIM-4 metallo-beta-lactamase, CTX-M-15 extended-spectrum beta-lactamase, and CMY-4 AmpC beta-lactamase in a Tunisian university hospital. *Antimicrob. Agents Chemother*. **2006**, *50*, 4198–4202.
(32) Mercuri, P. S.; Bouillenne, F.; Boschi, L.; Lamotte-Brasseur, J.; Amicosante, G.; Devreese, B.; Van Beeumen, J.; Frère, J. M.; Rossolini, G. M.; Galleni, M. Biochemical characterization of the FEZ-1 metallo-beta-lactamase of *Legionella gormanii* ATCC 33297T produced in *Escherichia coli*. *Antimicrob. Agents Chemother*. **2001**, *45*, 1254–1262.
(33) Lu, Y.; Shi, T.; Wang, Y.; Yang, H.; Yan, X.; Luo, X.; Jiang, H.; Zhu, W. Halogen bondings. A novel interaction for rational drug design? *J. Med. Chem*. **2009**, *52*, 2854–2862.
(34) Abrunhosa, I.; Drabowicz, J.; Grach, G.; Gulea, M.; Hamel, M.; Masson, S.; Mikolajczyk, M.; Vazeux, M. New chiral ortho-P,S-difunctionalized aromatic compounds. *Phosphorus, Sulfur Silicon Relat. Elem*. **2005**, *180*, 1267–1272.
(35) Gulea, M.; Hammerschmidt, F.; Marchand, P.; Masson, S.; Pisljagic, V.; Wuggenig, F. Synthesis of chiral, nonracemic alpha-sulfanylphosphonates and derivatives. *Tetrahedron: Asymmetry* **2003**, *14*, 1829–1836.
(36) McKenna, C. E.; Higa, M. T.; Cheung, N. H.; McKenna, M.-C. The facile dealkylation of phosphonic acid dialkyl esters by bromotrimethylsilane. *Tetrahedron Lett*. **1977**, *18*, 155–158.
(37) Masson, S.; Saint-Clair, J. F.; Saquet, M. Two methods for the synthesis of (2-mercaptophenyl)phosphonic acid. *Synthesis* **1993**, *5*, 485–486.
(38) Masson, S.; Saint-Clair, J. F.; Dore, A.; Saquet, M. Phosphorothioate−mercaptophosphonate rearrangement: synthesis of new *o*-mercaptoaryl- and *o*-mercaptoheteroaryl phosphonates and their derivatives. *Bull. Soc. Chim. Fr*. **1996**, *133*, 951–964.
(39) Bebrone, C.; Delbrück, H.; Kupper, M. B.; Schlömer, P.; Willmann, C.; Frère, J. M.; Fischer, R.; Galleni, M.; Hoffmann, K. M. The structure of the dizinc subclass B2 metallo-beta-lactamase CphA reveals that the second inhibitory zinc ion binds in the histidine site. *Antimicrob. Agents Chemother*. **2009**, *53*, 4464–4471.
(40) Garau, G.; Bebrone, C.; Anne, C.; Galleni, M.; Frère, J. M.; Dideberg, O. A Metallo-β-lactamase enzyme in action: crystal

structures of the monozinc carbapenemase CphA and its complex with biapenem. *J. Mol. Biol.* **2005**, *345*, 785–795.
(41) Bebrone, C.; Anne, C.; De Vriendt, K.; Devresse, B.; Van Beeumen, J.; Frère, J. M.; Galleni., M. Dramatic broadening of the substrate profile of the *Aeromonas hydrophila* CphA metallo-β-lactamase by site-directed mutagenesis. *J. Biol. Chem.* **2005**, *17*, 180–188.
(42) Damblon, C.; Jensen, M.; Ababou, A.; Barsukov, I.; Papamicael, C.; Schofield, C. J.; Olsen, L.; Bauer, R.; Roberts, G. C. The inhibitor thiomandelic acid binds to both metal ions in metallo-beta-lactamase and induces positive cooperativity in metal binding. *J. Biol. Chem.* **2003**, *278*, 29240–29251.
(43) Lassaux, P.; Traoré, D.A.K.; Loisel, E.; Favier, A.; Docquier, J. D.; Frère, J. M.; Ferrer, J. L.; Galleni, M. Biochemical and structural characterization of the subclass B1 metallo-beta-lactamase VIM-4. Unpublished results, 2009.
(44) Garcia-Saez, I.; Mercuri, P. S.; Papamicael, C.; Kahn, R.; Frère, J. M.; Galleni, M.; Rossolini, G. M.; Dideberg, O. Three-dimensional structure of FEZ-1, a monomeric subclass B3 metallo-beta-lactamase from *Fluoribacter gormanii*, in native form and in complex with D-captopril. *J. Mol. Biol.* **2003**, *325*, 651–660.
(45) Ullah, J. H.; Walsh, T. R.; Taylor, I. A.; Emery, D. C.; Verma, C. S.; Gamblin, S. J.; Spencer, J. The crystal structure of the L1 metallo-β-lactamase from *Stenotrophomonas maltophilia* at 1.7 Å resolution. *J. Mol. Biol.* **1998**, *284*, 125–136.
(46) Toney, J. H.; Fitzgerald, P. M.; Grover-Sharma, N.; Olson, S. H.; May, W. J.; Sundelof, J. G.; Vanderwall, D. E.; Cleary, K. A.; Grant, S. K.; Wu, J. K.; Kozarich, J. W.; Pompliano, D. L.; Hammond, G. G. Antibiotic sensitization using biphenyl tetrazoles as potent inhibitors of *Bacteroides fragilis* metallo-beta-lactamase. *Chem Biol.* **1998**, *5*, 185–196.
(47) Scrofani, S. D.; Chung, J.; Huntley, J. J.; Benkovic, S. J.; Wright, P. E.; Dyson, H. J. NMR characterization of the metallo-beta-lactamase from *Bacteroides fragilis* and its interaction with a tight-binding inhibitor: role of an active-site loop. *Biochemistry* **1999**, *38*, 14507–14514.
(48) Toney, J. H.; Hammond, G. G.; Fitzgerald, P. M.; Sharma, N.; Balkovec, J. M.; Rouen, G. P.; Olson, S. H.; Hammond, M. L.; Greenlee, M. L.; Gao, Y. D. Succinic acids as potent inhibitors of plasmid-borne IMP-1 metallo-beta-lactamase. *J. Biol. Chem.* **2001**, *276*, 31913–31918.
(49) Minond, D.; Saldanha, S. A.; Subramaniam, P.; Spaargaren, M.; Spicer, T.; Fotsing, J. R.; Weide, T.; Fokin, V. V.; Sharpless, K. B.; Galleni, M.; Bebrone, C.; Lassaux, P.; Hodder, P. Inhibitors of VIM-2 by screening pharmacologically active and click-chemistry compound libraries. *Bioorg. Med. Chem.* **2009**, *17*, 5027–5037.
(50) Horsfall, L. E.; Garau, G.; Liénard, B. M.; Dideberg, O.; Schofield, C. J.; Frère, J. M.; Galleni, M. Competitive inhibitors of the CphA metallo-β-lactamase from *Aeromonas hydrophila*. *Antimicrob. Agents Chemother.* **2007**, *51*, 2136–2142.
(51) Derewenda, Z. S.; Lee, L.; Derewenda, U. The occurrence of C−H···O hydrogen bonds in proteins. *J. Mol. Biol.* **1995**, *252*, 248–262.
(52) Crowder, M. W.; Walsh, T. R.; Banovic, L.; Pettit, M.; Spencer, J. Overexpression, purification, and characterization of the cloned metallo-beta-lactamase L1 from *Stenotrophomonas maltophilia*. *Antimicrob. Agents Chemother.* **1998**, *42*, 921–926.
(53) Cornish-Bowden, A. *Fundamentals of Enzyme Kinetics*; Portland Press Ltd.: London, 2001.
(54) Kabsch, W. Automatic processing of rotation diffraction data from crystals of initially unknown symmetry and cell constants. *J. Appl. Crystallogr.* **1993**, *26*, 795–800.
(55) CCP4 suite: programs for protein crystallography. *Acta Crystallogr., Sect. D* **1994**, *50*, 760−763.
(56) McCoy, A. J.; Grosse-Kunstleve, R. W.; Adams, P. D.; Winn, M. D.; Storoni, L. C.; Read, R. J. Phaser crystallographic software. *J. Appl. Crystallogr.* **2007**, *40*, 658–674.
(57) Perrakis, A.; Morris, R.; Lamzin, V. S. Automated protein model building combined with iterative structure refinement. *Nat. Struct. Biol.* **1999**, *6*, 458–463.
(58) Emsley, P.; Cowtan, K. Coot: model-building tools for molecular graphics. *Acta Crystallogr.* **2004**, *D60*, 2126–2132.
(59) Murshudov, G. N.; Vagin, A. A.; Dodson, E. J. Refinement of macromolecular structures by the maximum-likelihood method. *Acta Crystallogr.* **1997**, *D53*, 240–255.
(60) Programs InsightII 2000.3L and Discover; Accelrys Software Inc., www.accelrys.com.
(61) Bebrone, C.; Lassaux, P.; Vercheval, L.; Sohier, J. S.; Jehaes, A.; Sauvage, E.; Galleni, M. Current challenges in antimicrobial chemotherapy: focus on β-lactamase inhibition. *Drugs* **2010**, *70*, 651−679.
(62) Burkert, U.; Allinger, N. L. *Molecular Mechanics*; American Chemical Society: Washington, DC, 1982.
(63) Weiner, P. K.; Kollman, P. A. AMBER: assisted model building with energy refinement. A general program for modeling molecules and their interactions. *J. Comput. Chem.* **1981**, *2*, 287–303.
(64) Weiner, S. J.; Kollman, P. A.; Nguyen, D. T.; Case, D. A. An all atom force field for simulations of proteins and nucleic acids. *J. Comput. Chem.* **1986**, *7*, 230–252.
(65) Frisch, M. J.; Trucks, G. W.; Schlegel, H. B.; Scuseria, G. E.; Robb, M. A.; Cheeseman, J. R.; Montgomery, J. A., Jr.; Vreven, T.; Kudin, K. N.; Burant, J. C.; Millam, J. M.; Iyengar, S. S.; Tomasi, J.; Barone, V.; Mennucci, B.; Cossi, M.; Scalmani, G.; Rega, N.; Petersson, G. A.; Nakatsuji, H.; Hada, M.; Ehara, M.; Toyota, K.; Fukuda, R.; Hasegawa, J.; Ishida, M.; Nakajima, T.; Honda, Y.; Kitao, O.; Nakai, H.; Klene, M.; Li, X.; Knox, J. E.; Hratchian, H. P.; Cross, J. B.; Adamo, C.; Jaramillo, J.; Gomperts, R.; Stratmann, R. E.; Yazyev, O.; Austin, A. J.; Cammi, R.; Pomelli, C.; Ochterski, J. W.; Ayala, P. Y.; Morokuma, K.; Voth, G. A.; Salvador, P.; Dannenberg, J. J.; Zakrzewski, V. G.; Dapprich, S.; Daniels, A. D.; Strain, M. C.; Farkas, O.; Malick, D. K.; Rabuck, A. D.; Raghavachari, K.; Foresman, J. B.; Ortiz, J. V.; Cui, Q.; Baboul, A. G.; Clifford, S.; Cioslowski, J.; Stefanov, B. B.; Liu, G.; Liashenko, A.; Piskorz, P.; Komaromi, I.; Martin, R. L.; Fox, D. J.; Keith, T.; Al-Laham, M. A.; Peng, C. Y.; Nanayakkara, A.; Challacombe, M.; Gill, P. M. W.; Johnson, B.; Chen, W.; Wong, M. W.; Gonzalez, C. Pople, J. A. *Gaussian 03*, revision B.04; Gaussian, Inc.: Pittsburgh, PA, 2003.
(66) Wallace, A. C.; Laskowski, R. A.; Thornton, J. M. LIGPLOT: a program to generate schematic diagrams of protein−ligand interactions. *Protein Eng.* **1996**, *8*, 127–134.